

Numerical Simulations of Collisional Cascades at the Roche Limits of White Dwarf Stars

Scott J. Kenyon

Smithsonian Astrophysical Observatory, 60 Garden Street, Cambridge, MA 02138

e-mail: skenyon@cfa.harvard.edu

Benjamin C. Bromley

Department of Physics, University of Utah, 201 JFB, Salt Lake City, UT 84112

e-mail: bromley@physics.utah.edu

ABSTRACT

We consider the long-term collisional and dynamical evolution of solid material orbiting in a narrow annulus near the Roche limit of a white dwarf. With orbital velocities of 300 km s^{-1} , systems of solids with initial eccentricity $e \gtrsim 10^{-3}$ generate a collisional cascade where objects with radii $r \lesssim 100\text{--}300 \text{ km}$ are ground to dust. This process converts $1\text{--}100 \text{ km}$ asteroids into $1 \text{ }\mu\text{m}$ particles in $10^2\text{--}10^6 \text{ yr}$. Throughout this evolution, the swarm maintains an initially large vertical scale height H . Adding solids at a rate \dot{M} enables the system to find an equilibrium where the mass in solids is roughly constant. This equilibrium depends on \dot{M} and r_0 , the radius of the largest solid added to the swarm. When $r_0 \lesssim 10 \text{ km}$, this equilibrium is stable. For larger r_0 , the mass oscillates between high and low states; the fraction of time spent in high states ranges from 100% for large \dot{M} to much less than 1% for small \dot{M} . During high states, the stellar luminosity reprocessed by the solids is comparable to the excess infrared emission observed in many metallic line white dwarfs.

Subject headings: planetary systems – planets and satellites: formation – planets and satellites: physical evolution – planets and satellites: rings – stars: circumstellar matter – stars: white dwarfs

1. INTRODUCTION

Among nearby white dwarfs with H-rich (DA stars) or He-rich (DB stars) atmospheres, roughly 25% have metallic absorption lines from O, Mg, Al, Si, Ca, and Fe (e.g., Zuckerman

& Reid 1998; Zuckerman et al. 2010; Koester et al. 2014; Kepler et al. 2015, 2016; Farihi 2016, and references therein). Stars in the DZ class have strong metallic lines with little or no H or He (e.g., Sion et al. 1990; Koester et al. 2011; Sion et al. 2014; Kepler et al. 2015, 2016). A few per cent of these stars have near-IR excess emission from warm dust which reprocesses roughly 1% of the stellar luminosity (e.g., Kilic et al. 2005; Reach et al. 2005; Hansen et al. 2006; Kilic et al. 2006; Tremblay & Bergeron 2007; von Hippel et al. 2007; Kilic et al. 2008; Farihi et al. 2009; Girven et al. 2011; Debes et al. 2011; Chu et al. 2011; Girven et al. 2012; Barber et al. 2012; Hoard et al. 2013; Bergfors et al. 2014; Rocchetto et al. 2015; Barber et al. 2016; Bonsor et al. 2017). A few systems also have metallic emission features which sometimes display the characteristic double-peaked profile of a circumstellar disk (e.g., Gänsicke et al. 2006, 2007, 2008; Melis et al. 2010; Farihi et al. 2012; Melis et al. 2012; Debes et al. 2012a; Wilson et al. 2014).

Detailed models demonstrate that heavy metals in white dwarf atmospheres are continually replenished. Time scales for metals to diffuse from the atmosphere into the core are much shorter than the time scale for the white dwarf to cool (e.g., Fontaine & Michaud 1979; Alcock & Illarionov 1980; Lacombe et al. 1983; Wesemael et al. 1984; Dupuis et al. 1992; Althaus & Benvenuto 2000; Koester 2009). Explaining the observed abundances requires time-averaged accretion rates of $10^5 - 10^{12}$ g s⁻¹ for white dwarfs with ages of 0.1–3 Gyr (e.g., Koester & Wilken 2006; Deal et al. 2013; Koester et al. 2014; Farihi 2016). To put these rates in perspective, steady accretion at 10^{10} g s⁻¹ adds a km-sized object to the white dwarf every 2–3 weeks. Sustaining this rate for 1 Gyr requires a reservoir of 0.05 M_⊕ (see also Figs. 10–11 of Farihi 2016).

There are two sources for accreted material: the interstellar medium and solids leftover from a planetary system (e.g., Lacombe et al. 1983; Aannestad & Sion 1985; Alcock et al. 1986; Aannestad et al. 1993; Dupuis et al. 1993; Jura 2003; Koester & Wilken 2006; Jura et al. 2007b,a; Wyatt et al. 2014). As summarized in Farihi (2016), various observations rule out accretion from the ISM. In the current paradigm, solids on roughly circular orbits at large a survive the evolution of the central star into a red giant, ejection of a planetary nebula, and contraction into a white dwarf (e.g., Stern et al. 1990; Parriott & Alcock 1998; Debes & Sigurdsson 2002; Villaver & Livio 2007; Dong et al. 2010; Bonsor et al. 2011; Veras et al. 2013; Mustill et al. 2014). These solids are then somehow perturbed onto very high eccentricity ($e \gtrsim 0.99$) orbits which pass within the Roche limit of the white dwarf (e.g., Jura 2003, 2008; Debes et al. 2012b; Veras et al. 2013). Although the solids might hit the white dwarf directly, tidal forces probably disrupt the solids into myriad pieces which collide, fragment, and vaporize (see also Brown et al. 2017, and references therein). Over time, various physical processes somehow place material on nearly circular orbits close to the Roche limit, which then accretes onto the white dwarf.

Despite numerous investigations into the delivery of solids close to the white dwarf (e.g., Debes & Sigurdsson 2002; Veras & Gänsicke 2015; Bonsor & Veras 2015; Antoniadou & Veras 2016; Payne et al. 2017; Brown et al. 2017; Petrovich & Muñoz 2017) and the structure and evolution of solids and gas on circular orbits (e.g., Rafikov 2011a,b; Bochkarev & Rafikov 2011; Metzger et al. 2012; Rafikov & Garmilla 2012), few studies focus on the physical processes which convert very high e orbits into nearly circular orbits (see also Veras et al. 2014b, 2015b). Following tidal disruption, various processes – including collisions and gravitational stirring among the solids, vaporization, and interactions between the solids, the gas, and the stellar radiation field – change the orbits and physical properties of the solids. Currently, there is no single calculation which follows all of these processes in detail.

In this paper, we begin to consider how solid material on very high e orbits passing very close to a central white dwarf makes its way into the white dwarf photosphere. Because outcomes of various delivery models are uncertain, we study an idealized model where solids reside in a narrow annulus orbiting with initial eccentricity e_0 at the Roche limit. Our goal is to learn whether collisional and dynamical processes convert a system with non-zero e_0 into one with e very close to zero.

For this initial study, we perform a suite of numerical simulations which include *only* collisional and dynamical processes within the solids, Poynting-Robertson (PR) drag, and tidal interactions with the central star. Although these calculations ignore gas dynamics, simple estimates suggest gas drag probably has modest impact on the evolution. With this focus, we constrain the impact of collisional damping, dynamical friction, PR drag, and viscous stirring in setting the orbital properties of solids within the tidal field of the white dwarf.

Aside from establishing the long-term evolution of solids at the Roche limit, these calculations make initial predictions for the magnitude and behavior of IR excess emission as a function of the accretion rate and other properties of the solids. The second goal of this study is to begin to understand whether some aspects of our simulations can explain trends in the observations of metallic line white dwarfs.

Our investigation begins with some theoretical background to motivate the initial conditions for a suite of numerical calculations (§2). After describing our algorithms and summarizing our results (§3), we discuss the likely impact of gas dynamics and radiative processes, place our approach in context with other theoretical studies, make preliminary connections to observations, and outline future steps (§4). We conclude with a brief summary (§5).

2. THEORETICAL BACKGROUND

In the standard theoretical picture, solid fragments orbiting within the Roche limit dynamically relax into a flat disk (e.g., Debes & Sigurdsson 2002; Farihi 2016, and references therein). To avoid rapid depletion by PR drag, the disk is radially extended, vertically thin, and optically thick (e.g., Jura 2003; Rafikov 2011a; Farihi 2016). Adopting a radial temperature distribution for a flat disk, $T \propto r^{-3/4}$ (e.g., Friedjung 1985; Adams et al. 1987; Kenyon & Hartmann 1987; Chiang & Goldreich 1997), enables fits of model disk fluxes to observations of many systems with IR excesses (e.g., Jura 2003; Farihi 2016, and references therein). The small vertical extent of the disk, $H \approx 1$ cm to 1 m, implies a tiny vertical velocity dispersion, $v \lesssim 0.1$ cm s⁻¹; if $i/e = 0.5$, the orbital eccentricity, $e \lesssim 10^{-8}$. We want to learn whether ensembles of particles on eccentric orbits with $e \approx 10^{-3}$ –1 can reach the low e required by this model.

As a reasonable starting point for this discussion, we examine the evolution of solids orbiting near the Roche limit with initial eccentricity e_0 and inclination ι_0 . The solids have initial mass M_0 and an initial size distribution between a minimum radius r_{min} and a maximum radius r_0 . As the system evolves, additional solids are input at a rate \dot{M}_0 . These solids have radius r_0 and orbital parameters e_0 and ι_0 . Throughout the calculation, r_{min} is held fixed; the radius of the largest object in the grid, r_{max} , changes as collisions add or remove mass. Our goal is to establish outcomes of collisional evolution as a function of e_0 , r_0 , and \dot{M}_0 .

To set e_0 and ι_0 , we derive an orbital eccentricity e_V where high velocity collisions between solid particles vaporize a negligible amount of material. Unless gravitational interactions among the solids raise e and ι , starting with $e_0 \leq e_V$ and $\iota_0 = e_0/2$ ensures that collisions produce little or no gas throughout the evolution. The orbital velocity is $v_K = \sqrt{GM_{wd}/a} \approx 300$ –350 km s⁻¹ for white dwarf mass $M_{wd} = 0.6 M_\odot$ and semimajor axis $a \approx 1 R_\odot$. Simulations suggest collisions with impact velocities $\lesssim 3$ km s⁻¹ ($\gtrsim 30$ km s⁻¹) yield debris with a gas content $\lesssim 1\%$ ($\gtrsim 20\%$ –30%) of the initial mass (Tielens et al. 1994; Mann & Czechowski 2005; Czechowski & Mann 2007). Thus, we adopt $e_0 = e_V \approx 0.01$.

To set r_0 , we rely on data for asteroids in the solar system, which have radii ranging from 100–300 km to $\lesssim 0.5$ –1 km (e.g., Yoshida et al. 2003; Yoshida & Nakamura 2007; Gladman et al. 2009). To sample this range, we consider $r_0 = 0.1$ –100 km. As outlined below, sublimation probably sets a lower limit on the size of solid particles orbiting near the white dwarf, $r_{min} = 0.1$ –1 μm . Coagulation calculations are rarely sensitive to r_{min} , so we set $r_{min} = 1$ μm and do not consider other values. Our choices for \dot{M}_0 , 10^7 – 10^{13} g s⁻¹, are based on accretion rates inferred from the abundances of metals in white dwarf atmospheres,

$10^5 - 10^{12} \text{ g s}^{-1}$ (Farihi 2016, and references therein).

Although we expect r_0 and \dot{M}_0 to vary sporadically in a real system, these variables are held constant in each simulation. Setting $\dot{M}_0 = 0$ allows us to investigate systems where the mass flow rate through the cascade is much faster than the input rate. In calculations with $\dot{M}_0 \gg 0$, our goal is to learn whether the cascade finds a steady-state. Simulations over the complete range of \dot{M}_0 allow us to constrain time scales for evolving from one state to another and the detectability of cascades as a function of r_0 and \dot{M}_0 . The range we consider is sufficient to extrapolate results to other choices and to infer the impact of a time-varying r_0 or \dot{M}_0 .

2.1. Coagulation Code

To follow the evolution of rocky solid particles orbiting a white dwarf, we rely on *Orchestra*, a parallel C++/MPI hybrid coagulation + n -body code that tracks the accretion, fragmentation, and orbital evolution of solid particles ranging in size from a few microns to thousands of km (Kenyon 2002; Kenyon & Bromley 2008; Bromley & Kenyon 2011; Kenyon & Bromley 2016a; Kenyon et al. 2016). The ensemble of codes within *Orchestra* includes a multi-annulus coagulation code for small particles, an n -body code for large particles, and a radial diffusion code to follow the evolution of a gaseous circumstellar disk. Other algorithms link the codes together, enabling each component to react to the evolution of other components.

In this study, we assume particles lie within a single annulus of width Δa at a distance a from the central star ($\Delta a = 0.2a$). Within the annulus, there are M mass batches with characteristic mass m_i and logarithmic spacing $\delta = m_{i+1}/m_i$; adopting $\delta = 1.4$ provides a reasonably accurate solution for the cascade (e.g, Kenyon & Bromley 2015a,b, 2016a, and references therein). Batches contain N_i particles with total mass M_i , average mass $\bar{m}_i = M_i/N_i$, horizontal velocity h_i ($e_i = \sqrt{1.6}h_i/v_K$), and vertical velocity v_i ($\sin \iota = \sqrt{2}v_i/v_K$). The number of particles, total mass, and orbital velocity of each batch evolve through physical collisions and gravitational interactions with all other mass batches in the ring.

To specify collision rates, we adopt the particle-in-a-box algorithm. In this approach, the collision rate of all particles i with particles j is $\dot{N}_i = N_i N_j \sigma v f_g \epsilon/V$, where σ is the geometric cross-section, v is the relative velocity, f_g is the gravitational focusing factor, V is the volume occupied by the particles, and ϵ is a factor to avoid double counting when $i = j$ (Kenyon & Luu 1998; Kenyon & Bromley 2001, 2002). The relative velocity depends on

h_i and v_i . When relative velocities are large (small), f_g is derived in the dispersion (shear) regime with tidal effects included (Kenyon & Luu 1998; Kenyon & Bromley 2004a, 2012).

Collision outcomes depend on the ratio of the center-of-mass collision energy Q_c to the collision energy required to eject half of the mass to infinity Q_D^* . When two particles collide, the instantaneous mass of the merged particle is

$$m = m_i + m_j - m_{esc} , \quad (1)$$

where the mass of debris ejected in a collision is

$$m_{esc} = 0.5 (m_i + m_j) \left(\frac{Q_c}{Q_D^*} \right)^{b_d} , \quad (2)$$

the center-of-mass collision energy is

$$Q_c = \frac{m_i m_j v^2}{2 (m_i + m_j)^2} , \quad (3)$$

the binding energy of a merged pair of particles is (Benz & Asphaug 1999; Leinhardt & Stewart 2012)

$$Q_D^* = Q_b r^{\beta_b} + Q_g \rho_p r^{\beta_g} , \quad (4)$$

and b_d is a constant of order unity. In the expression for Q_D^* , the first (second) term corresponds to the bulk strength (gravity) component of the binding energy. We adopt $b_d = 1$ and set fragmentation parameters in the Q_D^* relation to those appropriate for rocky material: $Q_b \approx 3 \times 10^7 \text{ erg g}^{-1} \text{ cm}^{-\beta_b}$, $\beta_b \approx -0.40$, $Q_g \approx 0.3 \text{ erg g}^{-2} \text{ cm}^{3-\beta_g}$, and $\beta_g \approx 1.35$ for particles with mass density $\rho_p = 3 \text{ g cm}^{-3}$ (see also Davis et al. 1985; Holsapple 1994; Love & Ahrens 1996; Benz & Asphaug 1999; Housen & Holsapple 1999; Ryan et al. 1999; Arakawa et al. 2002; GIBLIN et al. 2004; Burchell et al. 2005). Particles in the debris have a power-law differential size distribution, $N(r) \propto r^{-3.5}$. The mass of the largest particle in the debris is

$$m_{max,d} = m_{L,0} \left(\frac{Q_c}{Q_D^*} \right)^{-b_L} m_{esc} , \quad (5)$$

$m_{L,0} \approx 0.01\text{--}0.5$, and $b_L \approx 0\text{--}1.25$ (Dohnanyi 1969; Wetherill & Stewart 1993; Williams & Wetherill 1994; O’Brien & Greenberg 2003; Kenyon & Bromley 2008; Kobayashi & Tanaka 2010; Weidenschilling 2010; Kenyon & Bromley 2016a). We adopt $m_{L,0} = 0.2$ and $b_L \approx 1$.

Near the Roche limit, the ability of colliding particles to merge into a larger particle depends on the tidal field of the white dwarf (e.g., Weidenschilling et al. 1984; Ohtsuki 1993; Canup & Esposito 1995; Karjalainen 2007; Porco et al. 2007; Tiscareno et al. 2013; Hyodo & Ohtsuki 2014; Yasui et al. 2014). We define the Hill radius

$$r_H = \left(\frac{m_i + m_j}{M_{wd}} \right)^{1/3} a , \quad (6)$$

which separates the volume where material is bound to the particles, $r \lesssim r_H$, from the volume where material is bound to the central star, $r \gtrsim r_H$. When the radius of the merged particle $r_s = r_i + r_j$ is smaller than r_H , the particles merge into a larger object. Otherwise, the collision results in two particles with total mass m from eq. (1). For convenience, we scale the mass lost from each particle by the initial mass, $m_{i,new} = m_i(1 - m_{esc}/(m_i + m_j))$.

The orbital elements e_i and i_i evolve due to collisional damping from inelastic collisions, gravitational interactions, and interactions with the radiation field of the central star. For inelastic and elastic collisions, we follow the statistical, Fokker-Planck approaches of Ohtsuki (1992) and Ohtsuki et al. (2002), which treat pairwise interactions (e.g., dynamical friction and viscous stirring) between all objects (see also Kenyon & Luu 1998; Kenyon & Bromley 2001, 2002, 2004a,b, 2008, 2015a, and references therein). For short-range interactions within 5–10 Hill radii, the Fokker-Planck formalism matches results from detailed n -body simulations. To treat interactions between solids with larger separations, we also calculate long-range stirring (Weidenschilling 1989). When the central star is a low luminosity white dwarf ($L_{wd} \lesssim 10^{-2} L_\odot$), radiation pressure has negligible impact on the orbital elements. However, we include radial drift and eccentricity damping from Poynting-Robertson drag (Burns et al. 1979). Our approach includes tidal terms appropriate for material within the Roche limit. Several test calculations with our algorithms reproduce results from previous studies of velocity evolution near the Roche limit (e.g., Canup & Esposito 1995; Ohtsuki 2000).

Throughout the evolution, collisional disruption generates particles with radii smaller than r_{min} , the smallest size included in the grid. We assume that these particles are removed by vaporization and do not interact with larger particles in the grid. Vaporized solids add material to a gaseous disk; over time, the gas accretes onto the white dwarf. We consider the likely impact of a gaseous on the solids in §4.2.

2.2. Tidal Disruption

Aside from treating tidal effects in collision outcomes and dynamical evolution, we must consider tidal disruption of solids near the Roche limit. Among various options for analyzing tidal stability (e.g., Aggarwal & Oberbeck 1974; Dobrovolskis 1990; Davidsson 1999, 2001), we infer constraints using failure criteria developed for terrestrial soils and applied to satellites of Mars and the giant planets in the solar system (e.g., Holsapple & Michel 2006, 2008; Sharma 2009, 2014). As in Holsapple & Michel (2006, 2008), we divide solids into small objects with finite cohesiveness and negligible self-gravity and large objects dominated by gravity. Approaches outlined in Sharma (2009, 2014) yield similar results.

For small objects, the upper limit of the spin periods of asteroids as a function of their measured diameter implies a cohesiveness $k = 2.25 \times 10^7 r^{-1/2}$ dyne cm^{-2} . Larger objects have smaller cohesiveness (more faults in their structure). Applying the Drucker-Prager model outlined in Holsapple & Michel (2008), we calculate $(a_d/R_{wd})(\rho/\rho_{wd})^{1/3}$, where a_d is the minimum stable distance for a solid with a given shape, spin, and mean density ρ orbiting a more massive central object with radius R_{wd} and mean density ρ_{wd} . For simplicity, we assume a spin axis parallel to the orbital axis.

Fig. 1 shows results for solids with $r = 1$ cm to 10 km. The dashed grey lines denote the classical Roche limit, a_R/R_{wd} , for fluids with $\rho = 3$ g cm^{-3} (upper curve) and $\rho = 6$ g cm^{-3} (lower curve) orbiting a $0.6 M_\odot$ white dwarf with a mean density¹ $\rho_{wd} = 4.45 \times 10^5$ g cm^{-3} , where

$$\frac{a_R}{R_{wd}} \approx C_R \left(\frac{\rho_{wd}}{10^6 \text{ g cm}^{-3}} \right)^{1/3} \left(\frac{3 \text{ g cm}^{-3}}{\rho} \right)^{1/3} \quad (7)$$

and $C_R \approx 170$. Adopting the standard cohesiveness (solid curves), solids with $r \leq 3$ –10 km are stable inside the classical Roche limit. Formally, particles with radii $r \leq 10$ m are stable even when they orbit at the surface of the white dwarf. Larger objects are progressively less stable until $r \approx 1$ –10 km, when the stability limit approaches the Roche limit. Prolate solids are more stable than spherical particles. Factor of ten smaller cohesiveness (dashed lines) has little impact on the results.

Other approaches to deriving the Roche limit for small solids yield fairly similar results. In his landmark paper, Jura (2003) adopted an expression for the Roche limit from Davidsson (1999) and set² the disruption radius a_d/R_{wd} as roughly 40% of a_R/R_{wd} . In more recent studies, $a_d \approx 80\%$ (Bear & Soker 2013) to 120% (Veras et al. 2014b) of a_R (see also Farihi 2016). All of these investigations assume the solids are rigid spheres, which tends to overestimate the disruption radius (e.g., Davidsson 1999, 2001; Holsapple & Michel 2008; Sharma 2014).

In the gravity limit, 10–100 km objects are probably also stable at $a_d \approx 0.5$ – $0.7 a_R$. In the solar system, the small satellites of Mars and the gas giants are tidally stable at approximately 2/3 of the standard fluid limit. To explain observations of eclipses in WD1145+017, Veras et al. (2017) simulated asteroid disruption with the N -body code PKDGRAV (e.g., Leinhardt et al. 2000; Richardson et al. 2000, 2005, and references therein). With $a \approx 0.7 a_R$,

¹To derive ρ_{wd} , we adopt the mass radius relation of Verbunt & Rappaport (1988). Other options yield similar results.

²Here, we correct for a factor of 10 overestimate of ρ_{wd} in Jura’s (2003) analysis, which places a_d for an asteroid outside a_R .

spherical objects with $r \approx 1\text{--}100$ km and $\rho \gtrsim 3$ g cm $^{-3}$ are stable against tidal disruption on 3 month to 2 yr time scales. Less dense solids disrupt within 1–30 days. For a fixed density, more massive asteroids are more stable.

Based on this discussion, we focus on the evolution of tidally stable objects with $r \leq 100$ km. Formally, tidally stable solids orbiting the white dwarf are prolate ellipsoids with aspect ratios of roughly 2:1:1. Tidal distortion has no impact on stirring rates, which depend on particle masses. Collision rates depend on geometric cross-sections, however, we ignore the slight changes in rates for ellipsoidal particles in this initial study.

2.3. Strategy for Numerical Simulations

In the next section, we consider a suite of numerical simulations designed to infer whether collisional evolution in systems of solids with $e_0 = 0.01$ and large vertical scale height leads to states with circular orbits and negligible vertical scale height. First, we demonstrate in §3.1 that swarms of *indestructible mono-disperse particles* with the cross-sectional area required to explain the IR excess emission of white dwarf debris disks damp on very short time scales.

We then consider a standard cascade calculation of a swarm of solids with initial mass M_0 and no input mass from external sources (§3.2). Although these systems also evolve rapidly, they never reach a state with small e and negligible v : collisional damping is negligible.

This failure motivates the model described in §3.3 where the input rate of solids is sufficient to balance the loss rate of particles with $r < r_{min}$. When the input particles are small, $r_{max} \lesssim 10\text{--}30$ km, collisional evolution yields an equilibrium mass proportional to the mass input rate \dot{M}_0 . Swarms with $r_{max} \gtrsim 10\text{--}30$ km cycle through periods of high mass and near-zero mass. The high mass limit of these swarms scales with \dot{M}_0 . Once again, though, the swarms never attain a state with small e and negligible vertical scale height.

3. NUMERICAL SIMULATIONS

To guide our interpretation of the calculations, we set several useful parameters. For an optically thin, vertically extended ring of debris, the luminosity reprocessed by small particles is $L_d/L_{wd} = A_d/4\pi a^2$ where A_d is the total cross-sectional area and a is the distance of the ring from the central star. Setting $a_0 \approx 1 R_\odot$ and $A_d \approx 10^{21}$ cm 2 yields $L_d/L_{wd} = 0.022$; observations indicate $L_d/L_{wd} \approx 10^{-3}\text{--}0.03$ (e.g., Barber et al. 2012; Hoard et al. 2013; Bergfors et al. 2014; Rocchetto et al. 2015; Barber et al. 2016; Farihi 2016, and references therein). If the debris consists of mono-disperse particles with radius r , the total mass is

$$M_d = 4\rho r A_d/3 = 1.33 \times 10^{21} \rho r \text{ g.}$$

As derived in Kenyon & Bromley (2016a), the collision time for a system of mono-disperse particles orbiting within a ring is $t_0 = r\rho P/12\pi\Sigma$, where ρ is the mass density, $P = 2\pi/\Omega$ is the orbital period, and $\Sigma = M_d/2\pi a\Delta a$ is the surface density (see also Kenyon et al. 2016, and references therein). This derivation assumes $f_g = 1$. For our standard ratio of M_d to A_d :

$$t_0 \approx 1.6 \times 10^3 \text{ s} \left(\frac{10^{21} \text{ cm}^2}{A_d} \right) \left(\frac{\Delta a}{0.2a} \right) \left(\frac{a}{1 R_\odot} \right)^{7/2} \quad (8)$$

Near the Roche limit, the collision time for mono-disperse particles with a detectable IR excess is roughly 10% of the orbital period around a $0.6 M_\odot$ white dwarf, $P = 1.3 \times 10^4 \text{ s} (a / 1 R_\odot)^{3/2}$.

When collisions produce a broad size distribution of particles, the collision time becomes smaller (Wyatt 2008; Kobayashi & Tanaka 2010; Wyatt et al. 2011; Kenyon & Bromley 2016a). Following previous studies, we set the collision time as $t_c = \alpha t_0$. In cascades where Q_D^* is independent of particle radius, v is the collision velocity, and $v^2/Q_D^* \gg 1$, $\alpha \approx 21(v^2/Q_D^*)^{-0.8}$ (Kenyon & Bromley 2017). White dwarf debris disks composed of 1 cm objects with $e \approx 0.01$ have $v^2/Q_D^* \approx 100$. The collision time t_c is then a factor of five smaller than the mono-disperse collision time t_0 .

For many conditions, PR drag operates on time scales much longer than physical collisions or gravitational stirring. Adopting relations for the time derivatives in semimajor axis, \dot{a} , and eccentricity, \dot{e} (Burns et al. 1979), the ratio $(\dot{e}/e) (a/\dot{a})$ is much smaller than 1 when $e \approx 1$ and somewhat larger than 1 when $e \approx 0$. In our simulations with $e \approx 0.01$, the time scale for radial drift is then roughly equal to the time scale for eccentricity damping:

$$t_{PR} \approx 5 \text{ yr} \left(\frac{r}{1 \mu\text{m}} \right) \left(\frac{a}{1 R_\odot} \right)^2 \left(\frac{10^{-2} L_\odot}{L_{wd}} \right). \quad (9)$$

When the surface density of solids becomes small, PR drag acts faster than collisions or gravitational stirring. For swarms of 1 μm (1 cm) particles, the $t_{PR} \approx t_0$ when $A_d \approx 10^{16} \text{ cm}^2$ ($A_d \approx 10^{12} \text{ cm}^2$) and $L_d/L_{wd} \approx 10^{-8}$ ($L_d/L_{wd} \approx 10^{-12}$). In our calculations, these conditions are rarely met; thus, PR drag has little influence on outcomes.

Once collisions produce debris, small grains may sublimate before interacting with other particles. Near the Sun, the sublimation time scale for 1 μm crystalline olivine grains is roughly 10 s at $8 R_\odot$, 10^3 s at $10 R_\odot$, and 10^5 s at $11 R_\odot$ (Kimura et al. 2002; Mann et al. 2004, 2006). Although amorphous olivine grains sublimate much more rapidly, pyroxene grains of any type sublimate much more slowly. Scaling these results to conditions appropriate for a white dwarf with an effective temperature $T_{wd} = 10^4 \text{ K}$, 1 μm crystalline olivine grains have

a sublimation time of roughly 10^5 s at the Roche limit. The time scale drops to 10^3 s when $a \approx 0.9a_R$. For comparison, pyroxene grains survive for $10^3 - 10^5$ s at $0.4-0.5 a_R$.

Although we do not know the grain type for debris disks around white dwarfs, these results suggest grains with $r \gtrsim 2-3 \mu\text{m}$ are safe from rapid sublimation at $0.5-1.0 a_R$. Much smaller grains with $r \lesssim 0.3 \mu\text{m}$ probably sublimate before they collide with another particle. In between these two size ranges, the grains are about as likely to sublimate as to collide with another grain. For simplicity, we assume that grains with $r \lesssim r_{min} = 1 \mu\text{m}$ sublimate as soon as they are formed.

3.1. Collisional Damping

To demonstrate how a swarm of solids *might* damp, we consider material³ with $A_d = 10^{21} \text{ cm}^2$ orbiting at $a = 0.71a_R = 1.15 R_\odot$ ($P = 4.5$ hr) around a $0.6 M_\odot$ white dwarf. In these test simulations, we follow a mono-disperse set of *indestructible* solids which evolve by collisional damping and viscous stirring.

Fig. 2 shows our results. With no change in particle properties, the evolution proceeds until (i) collisional damping and viscous stirring balance or (ii) the vertical scale height is equal to 1–2 particle radii. Although damping times for swarms with identical A_d are identical, larger particles stir the swarm faster than smaller particles. Thus, swarms of 1000 km particles find a balance with larger vertical scale height H than swarms of 1 cm particles. In this example, the equilibrium has $H \approx r$ and $e \approx 2 \times 10^{-11}r$.

As the vertical scale height of these rings approaches equilibrium, they are subject to gravitational instability (e.g., Goldreich & Ward 1973; Weidenschilling 1995; Youdin & Shu 2002; Chiang & Youdin 2010, and references therein). For a mono-disperse set of particles orbiting a $0.6 M_\odot$ white dwarf, the critical scale height for instability is

$$H_{crit} \approx 1 \text{ cm} \left(\frac{A_d}{10^{21} \text{ cm}^2} \right) \left(\frac{r}{1 \text{ cm}} \right) \left(\frac{\rho}{3 \text{ g cm}^{-3}} \right) \left(\frac{0.2a}{\Delta a} \right) \left(\frac{1 R_\odot}{a} \right)^{1/2}. \quad (10)$$

When $H \lesssim r$ $a \approx 1 R_\odot$, systems with $A_d \approx 10^{21} \text{ cm}^2$ tend to be unstable. Closer to the white dwarf, swarms with somewhat smaller A_d are also unstable.

At the Roche limit of a white dwarf, massive swarms of indestructible solids find an equilibrium with a vertical scale height comparable to the particle radius. Lower mass

³These choices are motivated by WD 1145+017 (Vanderburg et al. 2015), where solids with a large vertical scale height eclipse a central white dwarf.

swarms have larger H . For reasonable total masses, the maximum H is comparable to r for $r \lesssim 1\text{--}10$ cm and $\gtrsim 5\text{--}10 r$ for $r \gtrsim 10$ cm. Swarms of 1 cm or smaller particles with a total cross-sectional area large enough to produce an observable IR excess are probably gravitationally unstable. A system with enough mass in somewhat larger particles avoids the instability.

Although these results are encouraging, solid particles on high e orbits around a white dwarf are likely to suffer catastrophic collisions. We now consider whether systems with destructible particles can also find equilibria with small H .

3.2. Collisional Cascades with No Mass Input

Particles orbiting near the Roche limit of a white dwarf are fairly easy to break. We define an orbital eccentricity e_c required for catastrophic disruption, where the collision ejects half the mass of the combined mass of two colliding particles. For two equal mass objects with collision velocity $v \approx ev_K$, the center-of-mass collision energy is $Q_c = v^2/8 \approx e^2 v_k^2/8$. Setting $Q_c = Q_D^*$ (with Q_D^* from eq. 4) yields e_c . For our Q_D^* parameters, Fig. 3 shows e_c for orbits with $P = 4.5$ hr. Starting with $e_0 = 0.01$ guarantees catastrophic disruption of all solids with radii between 1 μm and 300 km.

To quantify the impact of destructive collisions on collisional damping, we follow the evolution of swarms with initial surface density $\Sigma_0 = 100$ g cm^{-2} and total mass $M_0 \approx 8 \times 10^{23}$ g in an annulus centered at $a = 1.15 R_\odot$ from a $0.6 M_\odot$ white dwarf. Material in this annulus has orbital period $P = 4.5$ hr, initial eccentricity $e_0 = 0.01$ and initial inclination $i_0 = e_0/2$. Calculations begin with a mono-disperse set of solids with initial radius r_0 .

Fig. 4 illustrates the time evolution of the total mass in solids. In each calculation, it takes 1–2 collision times to generate copious amounts of small objects which systematically remove mass from larger objects. Because the collision time is proportional to the cross-sectional area of the swarm, systems composed of 1 km and smaller objects evolve faster than systems of 100 km and smaller objects.

Initially, the mass drops monotonically with time. As the calculation proceeds, all systems end up with 1 or 2 large objects which dominate the mass of the swarm. If the debris can slowly grind down these objects, the mass continues to drop with time. Sometimes, however, the debris evolves more rapidly than the largest solids. The mass then remains roughly constant in time until the remaining large particles collide with each other (if there are at least two of them, as in the tracks for calculations with $r_0 = 10$ km and 30 km) or forever (if there is only one large object, as in the calculation with $r_0 = 100$ km).

While the mass in each system declines, collisional damping among small particles with $r \approx 1 \mu\text{m}$ to 10 cm overcomes stirring by the largest solids. However, the reduction in orbital e and i is rather small: e (i) drops from 0.01 (0.005) to 0.004–0.006 (0.002–0.003). At the end of these calculations, the vertical scale height $H \approx 1250\text{--}1500$ km is roughly 10% of the radius of the central white dwarf.

For a short period of time, there is enough debris in any of these systems to produce an observable IR excess (Fig. 5). When $r_0 = 1\text{--}3$ km, the IR luminosity maintains $L_d/L_{wd} = 0.01$ for 1–10 yr. After 100 yr, L_d/L_{wd} falls well below observed levels. For larger r_0 , the IR luminosity matches observed levels for 10–100 yr and then drops dramatically.

Occasional collisions among the largest objects produce the sporadic spikes in L_d/L_{wd} . In systems with larger r_0 , collisions among the largest objects are less frequent and produce more debris. Thus, the spikes in L_d/L_{wd} are more pronounced when r_0 is larger.

Throughout the period when the IR luminosity is $10^{-2} - 10^{-3} L_{wd}$, the production rate of $1 \mu\text{m}$ and smaller particles is $10^{12} - 10^{14} \text{ g s}^{-1}$. This rate is somewhat larger than the inferred accretion rates of solids onto metallic line white dwarfs. If the $1 \mu\text{m}$ and smaller particles sublimate, they will generate a gaseous ring which then expands into a disk. The rate of accretion onto the white dwarf depends on the viscous time scale and the underlying structure of the accretion disk. Deriving the rate of accretion onto the central white dwarf requires the solution of the radial diffusion equation for the gas (e.g., Metzger et al. 2012) which is beyond the scope of the present effort.

These calculations demonstrate that collisional damping is ineffective in reducing the vertical scale height of ensembles of solid particles with $r_0 = 1\text{--}100$ km and finite Q_D^* . Tests with $r_0 = 0.1\text{--}0.3$ km or $r_0 = 300\text{--}1000$ km yield similar results. Factor of three changes in Q_D^* also have modest impact on the evolution. Adopting smaller (larger) values for Q_D^* slows down (speeds up) the decline in M_d ; however, the overall character of the evolution is unchanged. In all cases, destructive collisions reduce the mass in solids to nearly zero before collisional damping can reduce the vertical scale height dramatically.

In these systems, the production rate of small particles and the dust luminosity are only briefly comparable with those required by observations. During these short periods, however, the evolution time is much shorter than typical time scales observed in metallic line white dwarfs.

3.3. Collisional Cascades with Mass Input

If the material lost to 1 μm particles is continuously re-supplied by an external source, it might be possible to maintain an equilibrium mass and luminosity for a ring of solid particles. In this equilibrium, the rate of mass input at the upper mass end of the cascade balances the rate the cascade generates solids with $r \leq r_{min}$. Defining \dot{M} as the mass loss rate through the cascade, $\dot{M} = M_d/t_c$. Using $t_c = \alpha t_0$, $M_{d,eq} = (\alpha r_0 \rho P a \Delta a \dot{M} / 6)^{1/2}$. To derive a simple closed form for the equilibrium mass in the gravity regime for Q_D^* with $r_0 \gtrsim 1$ km, we adopt representative values for other variables and set $e = 0.01$:

$$M_{d,eq} \approx 7 \times 10^{18} \text{ g} \left(\frac{\dot{M}}{10^{10} \text{ g s}^{-1}} \right)^{1/2} \left(\frac{0.6 M_\odot}{M_{wd}} \right)^{9/20} \left(\frac{r_0}{1 \text{ km}} \right)^{1.04} \left(\frac{\rho}{3 \text{ g cm}^{-3}} \right)^{9/10} \left(\frac{0.01}{e} \right)^{4/5} \left(\frac{\Delta a}{0.2a} \right)^{1/2} \left(\frac{a}{R_\odot} \right)^{43/20} \quad r_0 \gtrsim 1 \text{ km} . \quad (11)$$

The equilibrium mass is sensitive to the location of the ring. At fixed a , $M_{d,eq}$ varies roughly linearly with r_0 and as the square root of \dot{M} .

Maintaining this equilibrium requires that the time scale to replenish the ring, $t_r = M_{d,eq}/\dot{M}$, is not much longer than the collision time. For large objects and small \dot{M} , the mass in solids required to begin the cascade is large; t_r is also large. In these situations, we expect the ring to grow slowly in mass until the cascade begins; collisions then rapidly deplete the ring. The total mass oscillates.

As the evolution proceeds, the vertical scale height depends on the time scale for mass to flow from r_{max} to r_{min} . In most cascades, material flows from r_{max} to r_{min} in a few collision times. In some systems, however, there is enough mass in small particles for collisional damping to reduce the vertical scale height substantially (Kenyon & Bromley 2015a, 2016a,b). For rings of solids around white dwarfs, the most massive equilibrium rings require high input rates of massive particles. Thus, these systems have the best chance of developing the physical conditions that promote collisional damping.

To test these ideas, we consider the evolution of a ring of solids with initial mass $M_0 = 0$. Particles with radius r_0 , $e_0 = 0.01$, and $v_0 = e_0/2$ are added to the ring at a rate \dot{M}_0 . In each time step of length Δt , the number of particles with mass m_0 added to the grid is $\Delta N = \dot{M}_0 \Delta t / m_0$. Our algorithm uses a random number generator to round ΔN up or down to the nearest integer. For systems with large r_0 , this procedure introduces some shot noise into the input rate.

Each calculation follows the same pattern. Large solids are added to the swarm until they reach a critical cross-sectional area and begin to collide. Debris produced from the

first collision then interacts with all other particles in the grid. As this swarm evolves, large objects are continually added to the grid at the nominal rate \dot{M}_0 . These new objects continue to power the cascade.

Systems with small r_0 and large \dot{M}_0 easily attain an equilibrium where the mass and cross-sectional area of the swarm are roughly constant. In these calculations, there is little shot noise in the collision rate among the particles in the swarm or in the input rate of large objects. The equilibrium (M_d, A_d) depend on (r_0, \dot{M}_0) .

Fig. 6 shows the evolution in mass for systems with $r_0 = 1$ km ($m_0 \approx 10^{16}$ g). Swarms always find an equilibrium where the mass is nearly constant in time. Oscillations about this equilibrium mass are negligible (modest) for large (small) input rates. Shot noise produces these oscillations. At the lowest (highest) rates, a new object is added every 30 yr (20 min). At the lowest rates, a small degree of shot noise disrupts the smooth transport of mass from the largest to the smallest objects.

Systems with large r_0 and small \dot{M}_0 cannot find an equilibrium. Shot noise dominates the evolution. The swarm repeats a standard sequence of events, where (i) material is added until the cascade begins, (ii) the cross-sectional area rises dramatically, (iii) a robust cascade depletes the small particles in the swarm faster than collisions of large objects can replenish them, and (iv) A_d and to a lesser extent M_d decline dramatically. The duty cycle of this process depends on r_0 and the input rate. In these systems, the maximum mass is within a factor of ten of the equilibrium mass in eq. 11.

Fig. 7 repeats Fig. 6 for $r_0 = 100$ km ($m_0 \approx 10^{22}$ g). At the highest (lowest) input rates, an object is added every 30 yr (every 30 Myr). It takes 30–40 large objects to commence the cascade. The mass in solids is then sensitive to the input rate. At the largest rates, shot noise produces variations in the rate mass flows down the cascade. Thus, the equilibrium mass varies. At the lowest rates, the system gradually grows in mass until it has the requisite number of large objects to begin the cascade. Collisions then depletes the system at a rate much faster than the rate of adding large objects to the swarm. The mass drops and remains at some minimum level until the input of large objects raises the mass to the level required for a cascade.

When \dot{M}_0 is larger, the systems come closer to reaching an equilibrium. Large drops in the total mass become more and more infrequent. Once the input rate reaches 10^{12} g s⁻¹, the solids find a rough equilibrium with a mass close to the expected mass from eq. 11. Shot noise in the input rate generates fluctuations about the equilibrium.

For systems with large r_0 , all input \dot{M}_0 lead to roughly the same maximum mass in solids. This mass is close to the equilibrium mass for high input \dot{M}_0 . In these rings, the

mass in solids grows until the collision rate among the high mass objects reaches the rate required to power the cascade. This rate only depends on the cross-sectional area of the largest objects. While the rate is sensitive to r_0 , it is independent of \dot{M}_0 .

When $r_0 = 1\text{--}100$ km, the equilibrium disk mass agrees amazingly well with the analytical prediction (eq. 11). To make this comparison we examine the mass ratio $\xi = M_{eq,n}/M_{d,eq}$, where $M_{eq,n}$ is derived from simulations and $M_{d,eq}$ is the analytical prediction (eq. 11). For large r_0 , we consider only those calculations with large \dot{M}_0 where the fluctuations in the mass are small. Among 46 simulations with $\dot{M}_0 = 10^7 - 10^{13}$ g s⁻¹, $\xi = 2.0\text{--}2.5$ (Fig. 8); the average ratio is $\bar{\xi} = 2.19 \pm 0.15$. Despite the factor of two offset, the numerical simulations match the predicted variation of the equilibrium mass with \dot{M}_0 and r_0 . Considering the approximations made in deriving the analytical prediction, the good agreement is more than satisfactory.

Within a large suite of simulations with $r_0 = 0.1\text{--}300$ km and $\dot{M}_0 = 10^7 - 10^{13}$ g s⁻¹, collisional damping has negligible impact on the evolution. Fig. 9 shows an example of the evolution for $r_0 = 10$ km and $\dot{M}_0 = 10^{13}$ g s⁻¹. When the cascade begins, the solids have a vertical scale height $H = 2800$ km. As the simulation proceeds, large objects with $r \gtrsim 0.1\text{--}1$ km maintain this scale height. Collisional damping is ineffective. Although collisional damping often reduces the vertical scale height of small objects with $r \lesssim 1\text{--}10$ m, the reduction is modest. Once systems reach the equilibrium mass, small particles have $H \approx 1250\text{--}1750$ km. When systems cannot reach an equilibrium, collisional damping is more sporadic; $H \approx 2500\text{--}2800$ km.

In all simulations, the reprocessed luminosity of the particles L_d closely follows the total mass M_d . In Fig. 10, the predicted L_d/L_{wd} for systems with $r_0 = 1$ km rises when the solid mass reaches $M_d \approx 10^{18}$ g. Shortly thereafter, the luminosity finds an equilibrium with $L_d/L_{wd} \approx 10^{-3}(\dot{M}_0/10^{12} \text{ g s}^{-1})^{1/2}$. Systems with smaller \dot{M}_0 display larger fluctuations about this equilibrium luminosity.

Once $r_0 \gtrsim 100$ km, rings of solids with input $\dot{M}_0 \lesssim 10^{10}$ g s⁻¹ spend most of their time in a very low luminosity state with $L_d/L_{wd} \approx 10^{-8} - 10^{-7}$ (Fig. 11). During this period, the mass in large objects slowly grows. Eventually, the mass reaches a critical level of roughly 10^{23} g. Collisions then rapidly generate a luminous system, which quickly fades back to the faint minimum.

Rings with $r_0 = 100$ km and larger \dot{M}_0 attain a stable state where the luminosity fluctuates around a rough equilibrium. For any \dot{M}_0 , the typical luminosity is identical to the L_d/L_{wd} achieved by systems with smaller r_0 . However, the large flares in L_d/L_{wd} are much larger than those in rings with smaller r_0 .

To quantify how often these calculations generate detectable IR excesses, we define the detection probability as the fraction of time where the reprocessed luminosity $L_d/L_{wd} \gtrsim 10^{-3}$. Fig. 12 summarizes our results. At large \dot{M}_0 , systems with $r_0 = 1\text{--}100$ km spend nearly all of their time above the nominal detection limit. When $r_0 = 200\text{--}300$ km, the time required to accumulate enough mass for the cascade is a significant fraction of the evolution time. Thus, these systems are rarely detectable even when \dot{M}_0 is large.

For intermediate accretion rates, $\dot{M}_0 \approx 10^{11} - 10^{12}$ g s $^{-1}$, the detection probability is a few per cent. These systems spend more than 90% of their time in low states, where the cascade is fairly dormant. Once the cascade has enough mass, it briefly produces a detectable debris disk.

When the input \dot{M}_0 is small, the IR excess is rarely detectable. Cascades with $r_0 \lesssim 10$ km never generate enough mass in small particles to reach $L_d/L_{wd} = 10^{-3}$. Although systems with larger r_0 sometimes achieve large L_d/L_{wd} , the fraction of time spent in the bright state is small.

These results are remarkably independent of other input parameters in our calculations. The exponents b_d and b_l in our algorithms for debris production have a limited impact on M_d and L_d . Adopted values for Q_D^* are more important: increasing (reducing) Q_D^* slows down (speeds up) the conversion of particles with $r \lesssim 1$ km into smaller particles (Kobayashi & Tanaka 2010; Wyatt et al. 2011; Kenyon & Bromley 2016a, 2017). Thus, systems with smaller (larger) Q_D^* have smaller (larger) equilibrium values for M_d and L_d . For factor of three changes in Q_D^* , however, collisional damping still has negligible impact on the evolution. Cascades of destructive collisions of objects with $r_0 = 0.1\text{--}300$ km *always* prevent small particles from attaining a small vertical scale height.

4. DISCUSSION

Our calculations are the first to quantify the collisional evolution of massive rings of solid particles near the Roche limit of a white dwarf. Including accurate treatments for collision outcomes, dynamical interactions among the solids, and Poynting-Robertson drag, we derive the behavior of swarms as a function of various properties of the solids.

If ensembles of solids have no input from material outside the Roche limit, evolution is very rapid. In $\lesssim 10^3$ yr, collisions transform systems of 1–100 km objects with initial surface density $\Sigma_0 = 100$ g cm $^{-2}$ (mass $M_0 \approx 10^{24}$ g) and orbital eccentricity $e_0 = 0.01$ into 1 μ m particles which are swiftly vaporized into a metal-rich gas. Dynamical processes such as collisional damping, dynamical friction, Poynting-Robertson drag, and viscous stirring play

a minor role throughout the evolution.

Although choosing different initial masses for these systems changes the evolution time, long-term outcomes are identical. Eventually, cascades with $r_0 = 1\text{--}100$ km and $M_0 \lesssim 10^{25}$ g converge on the same size and velocity distributions. Dynamical processes remain unimportant.

Adding material to the ring at a constant rate \dot{M}_0 enables the system to reach an equilibrium where the mass of the swarm scales with $\dot{M}_0^{1/2}$ and r_0 . The equilibrium mass derived from numerical simulations is close to the predictions of a simple analytical model. For $r_0 \lesssim 10$ km, these equilibria are stable. Despite the roughly constant masses of these rings, dynamical processes still act on time scales much longer than the collision time. Thus, the vertical scale height H remains larger than r_0 . In systems with larger r_0 , the mass fluctuates by 1–10 orders of magnitude on time scales, $10^2 - 10^7$ yr, which depend on \dot{M}_0 . Dynamical processes are still relatively unimportant.

When rings of solids have an equilibrium mass and $\dot{M}_0 \gtrsim 10^{12}$ g s⁻¹, the stellar luminosity reprocessed by small particles is comparable to the luminosity of IR excess emission observed around many metallic line white dwarfs (Figs. 10–11). If \dot{M}_0 is smaller, adding large objects with $r_0 \gtrsim 30$ km to the swarm results in sporadic periods of large L_d/L_{wd} . The fraction of time spent with $L_d/L_{wd} \gtrsim 10^{-3}$ ranges from much less than 1% ($r_0 \gtrsim 30$ km, $\dot{M}_0 \lesssim 10^8$ g s⁻¹) to 10%–25% ($r_0 \gtrsim 30$ km, $\dot{M}_0 \approx 10^9 - 10^{11}$ g s⁻¹).

4.1. Collisional Damping in a Collisional Cascade

At first glance, the differences between Fig. 2 and Fig. 9 might seem remarkable. In systems with indestructible particles, damping reduces the vertical scale height by 50% in roughly ten collision times, $t_{50} \approx 10t_0 \approx 10^4$ s. Once collisions become destructive, damping is negligible.

However, destructible particles with $e_0 \approx 0.01$ do not survive long enough to damp. When two 1 cm particles with $e \approx 0.01$ collide, their center-of-mass collision energy is $Q_c \approx v^2/8 \approx 10^{10}$ erg g⁻¹. With $Q_D^* = 3 \times 10^7$ erg g⁻¹, $Q_c/Q_D^* \approx 375$; the particles are completely destroyed. From eq. 5, the radius of the largest particle in the debris is roughly 1 mm. The collision of two 1 mm particles yields material with sizes of 0.13 mm and smaller. It then takes another 3–4 collisions to reduce the debris to sub-micron sizes. Overall, the 5–6 collisions required to convert a pair of cm-sized particles into copious amounts of micron-sized particles is a factor of two smaller than the number of collisions required to damp their velocities by 50%.

Collisions can reduce the vertical scale height of large objects with mass m_1 after interactions with an equivalent mass in smaller objects (e.g., Goldreich et al. 2004). When these large objects orbit with $e \approx 0.01$ at the Roche limit of a white dwarf, however, they lose mass faster than they damp. For example, a 10 km (100 km) object colliding with a single smaller particle of mass m_2 loses a mass $\Delta m_1 \approx 10^3 m_2$ ($\Delta m_1 \approx 50 m_2$). Defining $N = m_1/m_2$ as the number of collisions required for the larger object to interact with an equivalent mass in smaller objects, it is clear that the total mass lost ($N\Delta m_1$) is much larger than m_1 .

Overall, the level of damping in Fig. 9 agrees with expectations based on the survival times. Over 5–6 collisions among small particles, we anticipate a 25% to 30% reduction in the scale height, which is reasonably close to the 33% reduction derived in the calculations. Because collisions with small particles rapidly destroy larger particles, damping of 1 m and larger particles should be smaller than that of smaller particles, as shown in Fig. 9. Once the mass in the annulus reaches a steady-state, the vertical scale height also reaches a steady-state which is set by the amount of damping achieved during the fairly short residence times of the small particles in the grid.

Compared to other situations where damping *has* been effective during a cascade (e.g., Kenyon & Bromley 2009, 2015a, 2016a,b), the Roche limit of a white dwarf is very harsh. At 1–100 AU, $e \approx 0.01$ produces modest ratios $Q_c/Q_D^* \approx 1 - 3$ instead of the $Q_c/Q_D^* \approx 100-1000$ discussed here. When $Q_c/Q_D^* \approx 1$, it takes $\gtrsim 25-50$ collisions to reduce a pair of 1 cm particles into sub-micron debris. If it takes 10 collisions to reduce the vertical scale height by a factor of two, there is a reasonable chance that damping can reduce the vertical scale height before particles are ground to dust. At the Roche limit, however, large and small particles are ground to sub-micron sizes much more rapidly than at 1–100 AU. Thus, damping is ineffective.

Since collisions and gravitational dynamics are unable to reduce H significantly, it is important to consider other physical processes capable of circularizing particle orbits. Within a protoplanetary disk, gas drag is a vital component of the growth of planetesimals into protoplanets (e.g., Youdin & Kenyon 2013). The Yarkovsky and YORP effects modify the orbits of asteroids and satellites in the solar system (e.g., Bottke et al. 2006). In the next two sub-sections, we examine whether any of these processes can circularize the orbits of particles involved in a cascade.

4.2. Reducing the Vertical Scale Height: Gas Drag

To estimate the impact of gas, we consider a simple model for a steady gaseous disk fed at a constant rate by the vaporization of 1 μm or smaller particles. The disk surface density $\Sigma_g = \dot{M}_0/3\pi\nu$ where $\nu = \alpha c_s H_g$ is the viscosity, α is the viscosity parameter, c_s is the sound speed, and H_g is the vertical scale height of the gas. Adopting $\alpha \approx 10^{-3}$ (Metzger et al. 2012) and a gas temperature $T_g = 4000$ K at $a \approx 1 R_\odot$ (e.g., Melis et al. 2010, 2012; Metzger et al. 2012), $c_s \approx 1$ km s $^{-1}$, $H_g \approx 2000$ km, and $\Sigma_g \approx 0.05$ g cm $^{-2}$ for $\dot{M}_0 = 10^{10}$ g s $^{-1}$. This estimate is similar to the $\Sigma_g \lesssim 0.01\text{--}0.1$ g cm $^{-2}$ derived in numerical simulations (e.g., Rafikov 2011b; Metzger et al. 2012).

In this example, the sound speed is comparable to the vertical velocity of solid particles. With $H_g \approx H_s$, solids spend most of their time interacting with the gas. For simplicity, we assume the solids ‘see’ a typical gas density, $\rho_g \approx \Sigma_g/H \approx 3 \times 10^{-10}$ g cm $^{-3}$. Factor of 2–3 changes in ρ_g have little impact on our discussion.

Within the gas, drag forces circularize the orbits of small particles (Adachi et al. 1976; Weidenschilling 1977; Rafikov 2004; Chiang & Youdin 2010; Youdin & Kenyon 2013). Defining F_d as the drag force, the ‘stopping time’ is $t_s = mv_g/F_d$, where v_g is the velocity of a particle relative to the gas. For small particles, we consider drag in the Epstein and Stokes regimes, which balance when the particle size $r \approx 9\lambda/4$, where $\lambda = \mu m_H c_s P/2\pi\Sigma_g\sigma_c$ is the mean free path, $\mu = 28$ is the mean molecular weight, and $\sigma_c = 5 \times 10^{-15}$ cm 2 is the collision cross-section for two Si atoms (Weidenschilling 1977; Rafikov 2004; Metzger et al. 2012). In our model disk, $\lambda \approx 4$ cm; drag is in the Epstein (Stokes) regime for $r \lesssim 4$ cm ($r \gtrsim 4$ cm). At 10 cm, the relevant stopping time is $t_s \approx 10^6$ s. The stopping time is comparable to the orbital period when $r \approx 1$ mm.

Knowledge of the stopping time allows us to assess the response of particles to the gas. When $\dot{M}_0 \approx 10^{10}$ g s $^{-1}$, particles with $r \approx 1$ mm encounter a mass in gas roughly equal to their own mass every orbital period. These and smaller ‘coupled’ particles become entrained in the gas and maintain a large vertical scale height. With velocities comparable to the sound speed, collisions between these particles are destructive and generate debris which remains coupled to the gas. Thus, the gas does not help to halt the cascade and reduce the vertical scale height of the smallest particles.

Although entrained particles drift radially, the drift time is longer than the collision time. For $\alpha = 10^{-3}$, the viscous time scale is roughly 10^3 yr. In our calculations, $t_c \lesssim 1\text{--}10$ yr. Thus, small particles undergo destructive collisions before they drift out of the ring.

Loosely coupled particles larger than 1 mm (i) drift radially inward and (ii) damp in

e and i . The gas has a finite pressure and orbits the central star at a lower velocity than solids on Keplerian orbits (Adachi et al. 1976; Weidenschilling 1977). Solids feel a ‘headwind’ which drags them inward and circularizes their orbits. Large particles with $r \gtrsim 10$ m feel little headwind and experience little radial drift or damping. The maximum radial drift rate for cm-sized to m-sized particles is the difference in orbital velocity between the gas and the solids. For metal-rich gas orbiting a white dwarf, this velocity is roughly 1 m s^{-1} (Metzger et al. 2012). The time scale to drift out of an annulus with width $\Delta a \approx 0.2a$ is several years. Orbits circularize on a similar time scale.

To estimate the relevance of radial drift and circularization, we compare the drift time scale to the collision time (eq. 8) and the time scale for the cascade to process small particles from 1–100 cm to $1 \mu\text{m}$ ($t_p \approx M_s/\dot{M}_0$, where M_s is the mass in small particles). For cascades with $r_0 = 1 \text{ km}$ and $\dot{M}_0 = 10^{10} \text{ g s}^{-1}$, $t_0 \approx 10^5 \text{ s}$ and $t_p \lesssim 10^6 \text{ s}$. The drift time scale is much longer than the collision time and somewhat longer than the processing time. Thus, it seems unlikely that gas drag has much impact on the cascade: collisions process small particles faster than the gas drags them inward.

For swarms with the equilibrium mass, $M_{d,eq}$, changing \dot{M}_0 is unlikely to modify these conclusions. Although the radial drift time is insensitive to the gas density, gaseous disks with larger \dot{M}_0 damp small particles more rapidly, $t_{damp} \propto \dot{M}_0^{-1}$. The collision and processing times scale as $\dot{M}_0^{-1/2}$. Systems with $\dot{M}_0 \lesssim 10^{10} \text{ g s}^{-1}$ are *less* susceptible to gas drag than those with larger \dot{M}_0 . When $\dot{M}_0 \approx 10^{14} \text{ g s}^{-1}$, $t_{damp} \approx t_c$. Although the gas might then circularize the orbits of small particles before collisions can destroy them, this \dot{M}_0 is much larger than the upper end of the range of observed \dot{M} in metallic line white dwarfs.

When $r_0 \gtrsim 30 \text{ km}$, the maximum mass is comparable to the equilibrium mass for a large \dot{M}_0 (Fig. 7). The ability of gas to reduce the vertical scale height of small particles then depends on how the gas and the solids interact during the short period of time when the cascade operates. Although evaluating the outcome requires a time-dependent calculation of the gas and the solids, our expectation is that the gas cannot reduce the vertical scale height of 1–100 cm particles before collisions them into mm and smaller particles which will become entrained in the gas and maintain a large vertical scale height.

Although improving our assessment requires more rigorous calculations of the gas, these results suggest that the gas has modest impact on the cascade. Combined with our earlier results, collisional dynamics, gas dynamics, and PR drag are unable to reduce the vertical scale height of solids from several thousand km to several km or several m.

4.3. Reducing the Vertical Scale Height: Other Options

Aside from radiation pressure and PR drag, other interactions between stellar radiation and small solids generate changes in a and e . In the Yarkovsky effect, differences in the loss of radiation from the hotter parts of a rotating solid relative to the cooler parts change a and to a lesser extent e (see the discussions in Burns et al. 1979; Bottke et al. 2006, and references therein). Differential radiation loss from the irregular surface of a solid (the YORP effect; Rubincam 2000, and references therein) modifies the spin rates of small solids and hence alters a and e . Although these effects change a and e on long time scales (Burns et al. 1979; Bottke et al. 2006; Veras et al. 2014a), they have negligible impact over the typical collision or processing time.

By analogy with the Yarkovsky and YORP effects, differential mass loss across the surface of a solid from sublimation might also induce \dot{a} and \dot{e} (Veras et al. 2015a). Rapid sublimation of ices from solids modify a and e on hundred year time scales. For systems dominated by collisions, however, all ices are probably liberated from the solids in a few collisions. Subsequent sublimation of the rocky material left behind occurs over much longer time scales.

Overall, radiation dynamics seems unlikely to reduce the vertical scale height of small solids orbiting at the Roche limit.

4.4. Shrinking Collisionless Rings

If these processes are unable to modify e and i significantly, it is necessary to identify other mechanisms. As one possibility, Veras et al. (2014b) consider tidal disruption of a spherical non-rotating asteroid passing within the Roche limit of the white dwarf (see also Richardson et al. 1998; Hahn & Rettig 1998; Scheeres et al. 2000; Sharma et al. 2006; Movshovitz et al. 2012). The asteroid has a rubble-pile structure with modest or negligible internal cohesion (e.g., Richardson et al. 2005; Sharma 2009). With these assumptions, asteroid disruption produces a set of distinct particles distributed along the original orbit of the asteroid. The system is then an eccentric, collisionless ring of small solid particles.

Once the ring forms, radiation from the central white dwarf shapes the dimensions of the ring (Veras et al. 2015b). For 1 cm particles with $e_0 = 0.99$ at $a_0 = 10$ AU, the time scale to drift inside $1 R_\odot$ is roughly $600 (r/1 \text{ cm}) (L_{wd}/10^{-2}L_\odot)^{-1}$ Myr (Burns et al. 1979; Veras et al. 2015b). As particles pass inside the Roche limit, they have $e_R \approx 0.01$. These outcomes are very sensitive to e_0 . When $e_0 = 0.999$ (0.98), the drift time drops (rises) to 20 Myr (1600 Myr) with $e_R \approx 0.16$ (0.004). For a typical white dwarf luminosity, 1 cm

particles that reach the Roche limit on a reasonable time scale have fairly eccentric orbits ($e \gtrsim 0.01$).

In these circumstances, collisional evolution of ring particles seems inevitable. At large a , particles on very eccentric orbits have shorter time scales for PR drag than for collisions. As a and e drop, t_0 gradually becomes shorter than t_{PR} (see eqs. 8–9). Although it is possible that ring particles maintain a collisionless structure inside the Roche limit, small differences in the properties of ring particles probably generate a modest dispersion in a , e , and i as the orbit contracts from $a \approx 10$ AU to $a \approx 1 R_\odot$. This dispersion leads to crossing orbits and collisional evolution.

As an example, tidally disrupting a single 1 km asteroid yields roughly 10^{16} 1 cm particles with a total cross-sectional area $A_d \approx 10^{16}$ cm². For orbits with $e \approx 0.01$ (0.1), $a \approx 1 R_\odot$, and $\Delta a \approx ea$, the collision time is a few months (a few yr; eq. 8), which is much shorter than the many centuries required for radiation to pull the solids into the sublimation radius. Because the collision time and the drag time both scale with particle radius, collisions always dominate.

From our calculations, rings of small particles with $e \gtrsim 10^{-3}$ produce a cascade which grinds solids into smaller and smaller objects. Although this evolution cannot modify e significantly, collisions try to puff up the inclinations of ring particles until $i \approx e/2$. The time scale for this change is 5–10 collision times, roughly the time to grind cm-sized to m-sized objects to dust.

4.5. Evolution of Solids: Alternative Treatments

To develop a better understanding of the relationship between solid particles and gas in white dwarf debris disks, Rafikov and collaborators investigated models where solids interact with the radiation field of the white dwarf and a gaseous circumstellar disk (Rafikov 2011a,b; Bochkarev & Rafikov 2011; Metzger et al. 2012; Rafikov & Garmilla 2012). In their picture, ensembles of small solids with $r \sim 1$ cm produced by tidal disruption of a single, much larger object follow circular orbits within a disk or ring inside the Roche limit. PR drag pulls these particles closer to the white dwarf, where the radiation field eventually vaporizes them. Vaporization generates a gaseous disk, which then interacts with the small particles through gas drag. On time scales somewhat longer than the viscous time of 10^3 yr, the system may develop phases of runaway accretion, where the rate gas falls onto the white dwarf grows dramatically with time. The runaway depletes the gaseous disk. If enough solids remain, this process can repeat; otherwise, a new runaway requires disruption of another large object.

In this approach, interactions among the small solids are minimal (see also Farihi et al. 2008). For cm-sized objects on circular orbits, collisional damping maintains low e and low z . Any low velocity collisions probably produce rebounds with little or no debris; mergers are rare. Although repeated rebounds gradually spread the ring, this process is slow. Under these conditions, there is little likelihood of a cascade or other rapid evolution of the solids.

From our calculations, attaining the initial configuration of this model seems challenging. Small solid particles generated from a disrupted asteroid or comet probably have modest e inside the Roche limit (e.g., Veras et al. 2015b). Once the orbits of these particles cross, a cascade is inevitable. The solids are then rapidly ground to dust and vaporized into a gas. From our estimates, mm-sized to cm-sized solids interacting with the gas do not drift very far from the cascade. Thus, it is hard to produce a swarm of small solids on nearly circular orbits.

Understanding the orbital geometry of solids inside the Roche limit requires more comprehensive calculations of the evolution of solids produced during the disruption of a comet or asteroid. If these solids can damp onto circular orbits before a cascade begins, then small particles can feed the structures envisioned in Rafikov & Garmilla (2012, and references therein) and generate gas which eventually accretes onto the central star. Otherwise, collisions are a more likely source of a gaseous disk.

4.6. Contacts with Observations

Despite the general failure in providing a clear path to disks with a small vertical scale height, cascade calculations of solids at the Roche limit enrich our understanding of metallic line white dwarfs. Although a disintegrating asteroid is a popular mechanism (e.g., Jura 2003, 2008; Bear & Soker 2013; Farihi et al. 2013; Vanderburg et al. 2015; Farihi 2016; Gurri et al. 2017, and references therein), cascades initiated by collisions of large asteroids (as investigated in §3) or by collisions of debris from a tidal disruption are a plausible alternative. Rather than attempt to explain observations, here we consider points of contact between our predictions and existing data. As we include more physical processes in the simulation, we plan more comprehensive comparisons with real systems.

- Dusty material with a large vertical extent is necessary to produce the broad range of eclipses in WD1145+017 (Vanderburg et al. 2015; Gänsicke et al. 2016; Alonso et al. 2016; Rappaport et al. 2016; Zhou et al. 2016; Croll et al. 2017; Gary et al. 2017; Hallakoun et al. 2017). In a cascade interpretation, eclipses result from small particles in the debris from high velocity collisions. Stochastic collisions lead to debris with variable

optical depth, accounting for short time scale variations in the system. Sublimation of particles with $r \lesssim 1 \mu\text{m}$ explains the presence of strong absorption features from a circumstellar gaseous disk. Entrainment of small particles within sublimating gas might account for plumes of material surrounding large objects. We plan additional calculations to consider this picture in more detail.

- In other systems, dust with a large vertical scale height can account for IR excess emission with reprocessed luminosity $L_d/L_{wd} \approx 10^{-3}$ to $3 - 4 \times 10^{-2}$ (e.g., Farihi 2016, and references therein). Cascades with high \dot{M}_0 or large r_0 account for these systems. Because these systems must wait to collect enough material to begin the cascade, models with large r_0 and a broad range of \dot{M}_0 naturally explain the low frequency of DBZ/DAZ/DZ white dwarfs with detectable IR excesses or gaseous disks. Our calculations predict stochastic changes in the IR excess with a broad range of amplitudes and time scales. Although we considered geometries where solids are confined to a narrow annulus, solids with a larger range in a probably follow a similar evolution (e.g., Kenyon & Bromley 2008, 2012; Kenyon et al. 2016).
- In the cascade picture, metallic line white dwarfs without IR excesses are systems with $\dot{M}_0 \lesssim 10^{11} \text{ g s}^{-1}$ or systems with $r_0 \gtrsim 30 \text{ km}$ in a ‘low’ state between periods of intense collisions. From our perspective, placing limits on the frequency of white dwarfs with circumstellar gas but no IR excess constrains models for sublimation of solids and viscous transport of the resulting gas.

4.7. Future Prospects

From our calculations, it seems possible to incorporate collisional cascades into the current framework for the formation and evolution of debris orbiting metallic line white dwarfs. As high eccentricity debris from disrupting asteroids or comets settles into lower e orbits, destructive collisions may play a useful role in generating a detectable IR excess. Gas from the vaporization of micron-sized particles within the cascade provides a path to produce the gaseous disks observed in many systems.

Developing a more robust model for cascades within the Roche limit requires addressing several issues. Solids with a large vertical scale height are hotter and more susceptible to rapid sublimation than solids in a disk with negligible vertical scale height (e.g., Jura 2003; Farihi 2016, and references therein). As discussed earlier, the magnitude of this effect depends on the vaporization time t_v relative to the collision time t_c and the time scale to replenish the cascade $t_r = M_d/\dot{M}_0$. In most of our calculations, $t_v \gg t_c$ and $t_v \ll t_r$. A proper

treatment of vaporization requires (i) identifying mechanisms to feed the cascade and (ii) a robust calculation of the evolution of the gas along with the evolution of the solids.

It is also important to consider outcomes for cascades outside the Roche limit. In our experience, collisional damping is effective at 0.1–2 AU (e.g., Kenyon & Bromley 2016a; Bromley & Kenyon 2017). Coupled with the larger equilibrium mass at larger a ($M_{d,eq} \propto a^{43/20}$, eq. 11) and the less restrictive conditions for growth by merger (Weidenschilling et al. 1984; Ohtsuki 1993; Canup & Esposito 1995; Porco et al. 2007), the cascade is probably less efficient and much less luminous at 2–3 a_R than at the Roche limit. Investigating outcomes for collisional evolution at 1–10 a_R would enable better comparisons between observations and numerical calculations.

Including the evolution of the gas in cascade calculations is another goal. Although our estimates suggest the gas has a modest impact on the cascade, inward drift of small particles entrained in the gas might increase the predicted magnitude of the IR excess relative to calculations without the gas.

We also need a better understanding of the orbits, shapes, sizes, and spin characteristics of solids scattered into orbits with periastra inside a_R . In many applications, collisional and dynamical evolution erases the initial state of the system; outcomes often have little relation to the initial conditions (e.g., Kenyon & Luu 1998; Kenyon & Bromley 2004a, 2008, 2010). In the calculations described here, the largest objects do not grow and dynamical evolution is negligible. Thus, outcomes are more sensitive to the initial e and ι of solid material. More robust predictions for the distribution of orbital parameters for solids would allow better tests of cascades models for white dwarf debris disks.

5. SUMMARY

We consider the collisional evolution of ensembles of asteroids orbiting within a narrow ring at the Roche limit of a low mass white dwarf. Solids with initial radius $r_0 = 1\text{--}100$ km and small eccentricity, $e \approx 0.01$, undergo a series of destructive collisions which grinds them to dust. As in other cascades, the dust luminosity declines roughly linearly with time (e.g., Wyatt & Dent 2002; Dominik & Decin 2003; Kenyon & Bromley 2004a; Wyatt 2008; Kenyon & Bromley 2016a, 2017).

When some physical process adds solids to the ring at a rate \dot{M}_0 , analytical results predict that the system evolves to an equilibrium mass which depends on \dot{M}_0 and the typical radius r_0 of large objects added to the ring (eq. 11). For $r_0 \lesssim 10$ km, numerical calculations confirm this result (Fig. 8). Adding larger objects to the ring leads to a system which (i)

maintains the equilibrium mass (for large \dot{M}_0) or (ii) oscillates between a very low mass and a high mass close to the equilibrium mass (for small \dot{M}_0).

Solid material in rings with $r_0 = 1\text{--}100$ km and total masses $M_d \approx 10^{20} - 10^{24}$ g evolve very rapidly. The typical time scale for collisions to convert sets of 1–100 km objects into 1 μm dust grains, $\lesssim 10\text{--}100$ yr, is often much shorter than the time scale for Poynting-Robertson drag to remove dust from the ring. During this evolution, dynamical processes do not act fast enough to change e and ι for solid particles.

Throughout the cascade, other processes also seem incapable of changing e and ι . The Yarkovsky and YORP effects modify e and ι on time scales much longer than the collision time. In cascades that generate significant amounts of gas, small particles with $r \lesssim 1$ mm are probably well-mixed with the gas. The large vertical scale height of the gas guarantees that small particles maintain large e and ι as they are ground to dust. The time scale for larger particles with $r \gtrsim 1$ mm to drift radially inward is long compared to the collision time. Thus, gas has little impact on the cascade.

These results indicate that collisional, gas dynamical, and radiative processes cannot significantly reduce the vertical scale height of swarms of solids with $H/R \gtrsim 0.01$ before a cascade grinds solids into small dust particles. If disks of small solid particles orbiting white dwarfs have negligible vertical scale height, either the particles arrive with negligible H or some other process circularizes their orbits.

Although it is premature to make detailed comparisons between the results of cascade calculations and data for DBZ/DAZ/DZ white dwarfs, it is encouraging that there are some points of contact between theoretical predictions and observations. The ability of cascades to maintain swarms of particles with large vertical scale height provides some hope for matching the IR excesses observed in many metallic line white dwarfs and the light curves of WD 1145+017. In cascades with large r_0 and \dot{M}_0 , intermittent IR excess emission may improve insight into the origin of the relatively low frequency of metallic white dwarfs with IR excesses or gaseous circumstellar disks and the apparent stochastic nature of metal accretion onto DA and DB white dwarfs (e.g., Wyatt et al. 2014; Bonsor et al. 2017).

Developing a more predictive theory of collisional cascades at the Roche limit requires (i) expanding the single annulus model to a multi-annulus model spanning a broader range of semimajor axes, (ii) including a prescription for evaporating/sublimating small solids into gas and following the evolution of the gas and solids together, and (iii) constructing algorithms for feeding the coagulation code with results from dynamical simulations. Applying our multi-annulus treatment of coagulation and gas dynamics to physical conditions near the Roche limit of a white dwarf is straightforward (e.g., Kenyon & Bromley 2008, 2010; Bromley

& Kenyon 2011, 2013; Kenyon & Bromley 2014). Currently, there are many theories for bringing solids to the white dwarf (e.g., Debes et al. 2012b; Frewen & Hansen 2014; Stone et al. 2015; Veras & Gänsicke 2015; Veras et al. 2015b,a; Payne et al. 2016; Antoniadou & Veras 2016; Payne et al. 2017). As these calculations mature, we plan to incorporate their approaches/results into our coagulation code.

We acknowledge a generous allotment of computer time on the NASA ‘discover’ cluster. Portions of this project were supported by the *NASA Outer Planets Program* through grant NNX11AM37G. We thank S. Rappaport for suggesting we study white dwarfs with metallic absorption lines. M. Payne provided a very useful set of comments which helped us improve the manuscript.

REFERENCES

- Aannestad, P. A., Kenyon, S. J., Hammond, G. L., & Sion, E. M. 1993, *AJ*, 105, 1033
- Aannestad, P. A., & Sion, E. M. 1985, *AJ*, 90, 1832
- Adachi, I., Hayashi, C., & Nakazawa, K. 1976, *Progress of Theoretical Physics*, 56, 1756
- Adams, F. C., Lada, C. J., & Shu, F. H. 1987, *ApJ*, 312, 788
- Aggarwal, H. R., & Oberbeck, V. R. 1974, *ApJ*, 191, 577
- Alcock, C., Fristrom, C. C., & Siegelman, R. 1986, *ApJ*, 302, 462
- Alcock, C., & Illarionov, A. 1980, *ApJ*, 235, 534
- Alonso, R., Rappaport, S., Deeg, H. J., & Palle, E. 2016, *A&A*, 589, L6
- Althaus, L. G., & Benvenuto, O. G. 2000, *MNRAS*, 317, 952
- Antoniadou, K. I., & Veras, D. 2016, *MNRAS*, 463, 4108
- Arakawa, M., Leliwa-Kopystynski, J., & Maeno, N. 2002, *Icarus*, 158, 516
- Barber, S. D., Belardi, C., Kilic, M., & Gianninas, A. 2016, *MNRAS*, 459, 1415
- Barber, S. D., Patterson, A. J., Kilic, M., et al. 2012, *ApJ*, 760, 26
- Bear, E., & Soker, N. 2013, *New A*, 19, 56
- Benz, W., & Asphaug, E. 1999, *Icarus*, 142, 5
- Bergfors, C., Farihi, J., Dufour, P., & Rocchetto, M. 2014, *MNRAS*, 444, 2147
- Bochkarev, K. V., & Rafikov, R. R. 2011, *ApJ*, 741, 36
- Bonsor, A., Farihi, J., Wyatt, M. C., & van Lieshout, R. 2017, *MNRAS*, 468, 154
- Bonsor, A., Mustill, A. J., & Wyatt, M. C. 2011, *MNRAS*, 414, 930
- Bonsor, A., & Veras, D. 2015, *MNRAS*, 454, 53
- Bottke, Jr., W. F., Vokrouhlický, D., Rubincam, D. P., & Nesvorný, D. 2006, *Annual Review of Earth and Planetary Sciences*, 34, 157
- Bromley, B. C., & Kenyon, S. J. 2011, *ApJ*, 731, 101

- . 2013, *ApJ*, 764, 192
- . 2017, *AJ*, 153, 216
- Brown, J. C., Veras, D., & Gaensicke, B. T. 2017, *MNRAS*, 468, 1575
- Burchell, M. J., Leliwa-Kopystyński, J., & Arakawa, M. 2005, *Icarus*, 179, 274
- Burns, J. A., Lamy, P. L., & Soter, S. 1979, *Icarus*, 40, 1
- Canup, R. M., & Esposito, L. W. 1995, *Icarus*, 113, 331
- Chiang, E., & Youdin, A. N. 2010, *Annual Review of Earth and Planetary Sciences*, 38, 493
- Chiang, E. I., & Goldreich, P. 1997, *ApJ*, 490, 368
- Chu, Y.-H., Su, K. Y. L., Bilikova, J., et al. 2011, *AJ*, 142, 75
- Croll, B., Dalba, P. A., Vanderburg, A., et al. 2017, *ApJ*, 836, 82
- Czechowski, A., & Mann, I. 2007, *ApJ*, 660, 1541
- Davidsson, B. J. R. 1999, *Icarus*, 142, 525
- . 2001, *Icarus*, 149, 375
- Davis, D. R., Chapman, C. R., Weidenschilling, S. J., & Greenberg, R. 1985, *Icarus*, 63, 30
- Deal, M., Deheuvels, S., Vauclair, G., Vauclair, S., & Wachlin, F. C. 2013, *A&A*, 557, L12
- Debes, J. H., Hoard, D. W., Wachter, S., Leisawitz, D. T., & Cohen, M. 2011, *ApJS*, 197, 38
- Debes, J. H., Kilic, M., Faedi, F., et al. 2012a, *ApJ*, 754, 59
- Debes, J. H., & Sigurdsson, S. 2002, *ApJ*, 572, 556
- Debes, J. H., Walsh, K. J., & Stark, C. 2012b, *ApJ*, 747, 148
- Dobrovolskis, A. R. 1990, *Icarus*, 88, 24
- Dohnanyi, J. S. 1969, *J. Geophys. Res.*, 74, 2531
- Dominik, C., & Decin, G. 2003, *ApJ*, 598, 626
- Dong, R., Wang, Y., Lin, D. N. C., & Liu, X.-W. 2010, *ApJ*, 715, 1036

- Dupuis, J., Fontaine, G., Pelletier, C., & Wesemael, F. 1992, *ApJS*, 82, 505
- Dupuis, J., Fontaine, G., & Wesemael, F. 1993, *ApJS*, 87, 345
- Farihi, J. 2016, *New A Rev.*, 71, 9
- Farihi, J., Gänsicke, B. T., & Koester, D. 2013, *Science*, 342, 218
- Farihi, J., Gänsicke, B. T., Steele, P. R., et al. 2012, *MNRAS*, 421, 1635
- Farihi, J., Jura, M., & Zuckerman, B. 2009, *ApJ*, 694, 805
- Farihi, J., Zuckerman, B., & Becklin, E. E. 2008, *ApJ*, 674, 431
- Fontaine, G., & Michaud, G. 1979, *ApJ*, 231, 826
- Frewen, S. F. N., & Hansen, B. M. S. 2014, *MNRAS*, 439, 2442
- Friedjung, M. 1985, *A&A*, 146, 366
- Gänsicke, B. T., Koester, D., Marsh, T. R., Rebassa-Mansergas, A., & Southworth, J. 2008, *MNRAS*, 391, L103
- Gänsicke, B. T., Marsh, T. R., & Southworth, J. 2007, *MNRAS*, 380, L35
- Gänsicke, B. T., Marsh, T. R., Southworth, J., & Rebassa-Mansergas, A. 2006, *Science*, 314, 1908
- Gänsicke, B. T., Aungwerojwit, A., Marsh, T. R., et al. 2016, *ApJ*, 818, L7
- Gary, B. L., Rappaport, S., Kaye, T. G., Alonso, R., & Hambachs, F.-J. 2017, *MNRAS*, 465, 3267
- Giblin, I., Davis, D. R., & Ryan, E. V. 2004, *Icarus*, 171, 487
- Girven, J., Brinkworth, C. S., Farihi, J., et al. 2012, *ApJ*, 749, 154
- Girven, J., Gänsicke, B. T., Steeghs, D., & Koester, D. 2011, *MNRAS*, 417, 1210
- Gladman, B. J., Davis, D. R., Neese, C., et al. 2009, *Icarus*, 202, 104
- Goldreich, P., Lithwick, Y., & Sari, R. 2004, *ARA&A*, 42, 549
- Goldreich, P., & Ward, W. R. 1973, *ApJ*, 183, 1051
- Gurri, P., Veras, D., & Gänsicke, B. T. 2017, *MNRAS*, 464, 321

- Hahn, J. M., & Rettig, T. W. 1998, *Planet. Space Sci.*, 46, 1677
- Hallakoun, N., Xu, S., Maoz, D., et al. 2017, *ArXiv e-prints*, arXiv:1702.05483
- Hansen, B. M. S., Kulkarni, S., & Wiktorowicz, S. 2006, *AJ*, 131, 1106
- Hoard, D. W., Debes, J. H., Wachter, S., Leisawitz, D. T., & Cohen, M. 2013, *ApJ*, 770, 21
- Holsapple, K. A. 1994, *Planet. Space Sci.*, 42, 1067
- Holsapple, K. A., & Michel, P. 2006, *Icarus*, 183, 331
- . 2008, *Icarus*, 193, 283
- Housen, K. R., & Holsapple, K. A. 1999, *Icarus*, 142, 21
- Hyodo, R., & Ohtsuki, K. 2014, *ApJ*, 787, 56
- Jura, M. 2003, *ApJ*, 584, L91
- . 2008, *AJ*, 135, 1785
- Jura, M., Farihi, J., & Zuckerman, B. 2007a, *ApJ*, 663, 1285
- Jura, M., Farihi, J., Zuckerman, B., & Becklin, E. E. 2007b, *AJ*, 133, 1927
- Karjalainen, R. 2007, *Icarus*, 189, 523
- Kenyon, S. J. 2002, *PASP*, 114, 265
- Kenyon, S. J., & Bromley, B. C. 2001, *AJ*, 121, 538
- . 2002, *AJ*, 123, 1757
- . 2004a, *AJ*, 127, 513
- . 2004b, *AJ*, 128, 1916
- . 2008, *ApJS*, 179, 451
- . 2009, *ApJ*, 690, L140
- . 2010, *ApJS*, 188, 242
- . 2012, *AJ*, 143, 63
- . 2014, *AJ*, 147, 8

- . 2015a, *ApJ*, 806, 42
- . 2015b, *ApJ*, 811, 60
- . 2016a, *ApJ*, 817, 51
- . 2016b, *ApJ*, 825, 33
- . 2017, *ApJ*, 839, 38
- Kenyon, S. J., & Hartmann, L. 1987, *ApJ*, 323, 714
- Kenyon, S. J., & Luu, J. X. 1998, *AJ*, 115, 2136
- Kenyon, S. J., Najita, J. R., & Bromley, B. C. 2016, *ApJ*, 831, 8
- Kepler, S. O., Pelisoli, I., Koester, D., et al. 2015, *MNRAS*, 446, 4078
- . 2016, *MNRAS*, 455, 3413
- Kilic, M., Farihi, J., Nitta, A., & Leggett, S. K. 2008, *AJ*, 136, 111
- Kilic, M., von Hippel, T., Leggett, S. K., & Winget, D. E. 2005, *ApJ*, 632, L115
- . 2006, *ApJ*, 646, 474
- Kimura, H., Mann, I., Biesecker, D. A., & Jessberger, E. K. 2002, *Icarus*, 159, 529
- Kobayashi, H., & Tanaka, H. 2010, *Icarus*, 206, 735
- Koester, D. 2009, *A&A*, 498, 517
- Koester, D., Gänsicke, B. T., & Farihi, J. 2014, *A&A*, 566, A34
- Koester, D., Girven, J., Gänsicke, B. T., & Dufour, P. 2011, *A&A*, 530, A114
- Koester, D., & Wilken, D. 2006, *A&A*, 453, 1051
- Lacombe, P., Wesemael, F., Fontaine, G., & Liebert, J. 1983, *ApJ*, 272, 660
- Leinhardt, Z. M., Richardson, D. C., & Quinn, T. 2000, *Icarus*, 146, 133
- Leinhardt, Z. M., & Stewart, S. T. 2012, *ApJ*, 745, 79
- Love, S. G., & Ahrens, T. J. 1996, *Icarus*, 124, 141
- Mann, I., & Czechowski, A. 2005, *ApJ*, 621, L73

- Mann, I., Köhler, M., Kimura, H., Cechowski, A., & Minato, T. 2006, *A&A Rev.*, 13, 159
- Mann, I., Kimura, H., Biesecker, D. A., et al. 2004, *Space Sci. Rev.*, 110, 269
- Melis, C., Jura, M., Albert, L., Klein, B., & Zuckerman, B. 2010, *ApJ*, 722, 1078
- Melis, C., Dufour, P., Farihi, J., et al. 2012, *ApJ*, 751, L4
- Metzger, B. D., Rafikov, R. R., & Bochkarev, K. V. 2012, *MNRAS*, 423, 505
- Movshovitz, N., Asphaug, E., & Korycansky, D. 2012, *ApJ*, 759, 93
- Mustill, A. J., Veras, D., & Villaver, E. 2014, *MNRAS*, 437, 1404
- O’Brien, D. P., & Greenberg, R. 2003, *Icarus*, 164, 334
- Ohtsuki, K. 1992, *Icarus*, 98, 20
- . 1993, *Icarus*, 106, 228
- . 2000, *Planet. Space Sci.*, 48, 553
- Ohtsuki, K., Stewart, G. R., & Ida, S. 2002, *Icarus*, 155, 436
- Parriott, J., & Alcock, C. 1998, *ApJ*, 501, 357
- Payne, M. J., Veras, D., Gänsicke, B. T., & Holman, M. J. 2017, *MNRAS*, 464, 2557
- Payne, M. J., Veras, D., Holman, M. J., & Gänsicke, B. T. 2016, *MNRAS*, 457, 217
- Petrovich, C., & Muñoz, D. J. 2017, *ApJ*, 834, 116
- Porco, C. C., Thomas, P. C., Weiss, J. W., & Richardson, D. C. 2007, *Science*, 318, 1602
- Rafikov, R. R. 2004, *AJ*, 128, 1348
- . 2011a, *ApJ*, 732, L3
- . 2011b, *MNRAS*, 416, L55
- Rafikov, R. R., & Garmilla, J. A. 2012, *ApJ*, 760, 123
- Rappaport, S., Gary, B. L., Kaye, T., et al. 2016, *MNRAS*, 458, 3904
- Reach, W. T., Kuchner, M. J., von Hippel, T., et al. 2005, *ApJ*, 635, L161
- Richardson, D. C., Bottke, W. F., & Love, S. G. 1998, *Icarus*, 134, 47

- Richardson, D. C., Elankumaran, P., & Sanderson, R. E. 2005, *Icarus*, 173, 349
- Richardson, D. C., Quinn, T., Stadel, J., & Lake, G. 2000, *Icarus*, 143, 45
- Rocchetto, M., Farihi, J., Gänsicke, B. T., & Bergfors, C. 2015, *MNRAS*, 449, 574
- Rubincam, D. P. 2000, *Icarus*, 148, 2
- Ryan, E. V., Davis, D. R., & Giblin, I. 1999, *Icarus*, 142, 56
- Scheeres, D. J., Ostro, S. J., Werner, R. A., Asphaug, E., & Hudson, R. S. 2000, *Icarus*, 147, 106
- Sharma, I. 2009, *Icarus*, 200, 636
- . 2014, *Icarus*, 229, 278
- Sharma, I., Jenkins, J. T., & Burns, J. A. 2006, *Icarus*, 183, 312
- Sion, E. M., Holberg, J. B., Oswalt, T. D., et al. 2014, *AJ*, 147, 129
- Sion, E. M., Kenyon, S. J., & Aannestad, P. A. 1990, *ApJS*, 72, 707
- Stern, S. A., Shull, J. M., & Brandt, J. C. 1990, *Nature*, 345, 305
- Stone, N., Metzger, B. D., & Loeb, A. 2015, *MNRAS*, 448, 188
- Tielens, A. G. G. M., McKee, C. F., Seab, C. G., & Hollenbach, D. J. 1994, *ApJ*, 431, 321
- Tiscareno, M. S., Hedman, M. M., Burns, J. A., & Castillo-Rogez, J. 2013, *ApJ*, 765, L28
- Tremblay, P.-E., & Bergeron, P. 2007, *ApJ*, 657, 1013
- Vanderburg, A., Johnson, J. A., Rappaport, S., et al. 2015, *Nature*, 526, 546
- Veras, D., Carter, P. J., Leinhardt, Z. M., & Gänsicke, B. T. 2017, *MNRAS*, 465, 1008
- Veras, D., Eggl, S., & Gänsicke, B. T. 2015a, *MNRAS*, 452, 1945
- Veras, D., & Gänsicke, B. T. 2015, *MNRAS*, 447, 1049
- Veras, D., Jacobson, S. A., & Gänsicke, B. T. 2014a, *MNRAS*, 445, 2794
- Veras, D., Leinhardt, Z. M., Bonsor, A., & Gänsicke, B. T. 2014b, *MNRAS*, 445, 2244
- Veras, D., Leinhardt, Z. M., Eggl, S., & Gänsicke, B. T. 2015b, *MNRAS*, 451, 3453

- Veras, D., Mustill, A. J., Bonsor, A., & Wyatt, M. C. 2013, *MNRAS*, 431, 1686
- Verbunt, F., & Rappaport, S. 1988, *ApJ*, 332, 193
- Villaver, E., & Livio, M. 2007, *ApJ*, 661, 1192
- von Hippel, T., Kuchner, M. J., Kilic, M., Mullally, F., & Reach, W. T. 2007, *ApJ*, 662, 544
- Weidenschilling, S. J. 1977, *MNRAS*, 180, 57
- . 1989, *Icarus*, 80, 179
- . 1995, *Icarus*, 116, 433
- . 2010, *ApJ*, 722, 1716
- Weidenschilling, S. J., Chapman, C. R., Davis, D. R., & Greenberg, R. 1984, in *IAU Colloq. 75: Planetary Rings*, ed. R. Greenberg & A. Brahic, 367–415
- Wesemael, F., Henry, R. B. C., & Shipman, H. L. 1984, *ApJ*, 287, 868
- Wetherill, G. W., & Stewart, G. R. 1993, *Icarus*, 106, 190
- Williams, D. R., & Wetherill, G. W. 1994, *Icarus*, 107, 117
- Wilson, D. J., Gänsicke, B. T., Koester, D., et al. 2014, *MNRAS*, 445, 1878
- Wyatt, M. C. 2008, *ARA&A*, 46, 339
- Wyatt, M. C., Clarke, C. J., & Booth, M. 2011, *Celestial Mechanics and Dynamical Astronomy*, 111, 1
- Wyatt, M. C., & Dent, W. R. F. 2002, *MNRAS*, 334, 589
- Wyatt, M. C., Farihi, J., Pringle, J. E., & Bonsor, A. 2014, *MNRAS*, 439, 3371
- Yasui, Y., Ohtsuki, K., & Daisaka, H. 2014, *ApJ*, 797, 93
- Yoshida, F., & Nakamura, T. 2007, *Planet. Space Sci.*, 55, 1113
- Yoshida, F., Nakamura, T., Watanabe, J., et al. 2003, *PASJ*, 55, 701
- Youdin, A. N., & Kenyon, S. J. 2013, *From Disks to Planets*, ed. T. D. Oswalt, L. M. French, & P. Kalas (Dordrecht: Springer Science & Business Media), 1
- Youdin, A. N., & Shu, F. H. 2002, *ApJ*, 580, 494

Zhou, G., Kedziora-Chudczer, L., Bailey, J., et al. 2016, MNRAS, 463, 4422

Zuckerman, B., Melis, C., Klein, B., Koester, D., & Jura, M. 2010, ApJ, 722, 725

Zuckerman, B., & Reid, I. N. 1998, ApJ, 505, L143

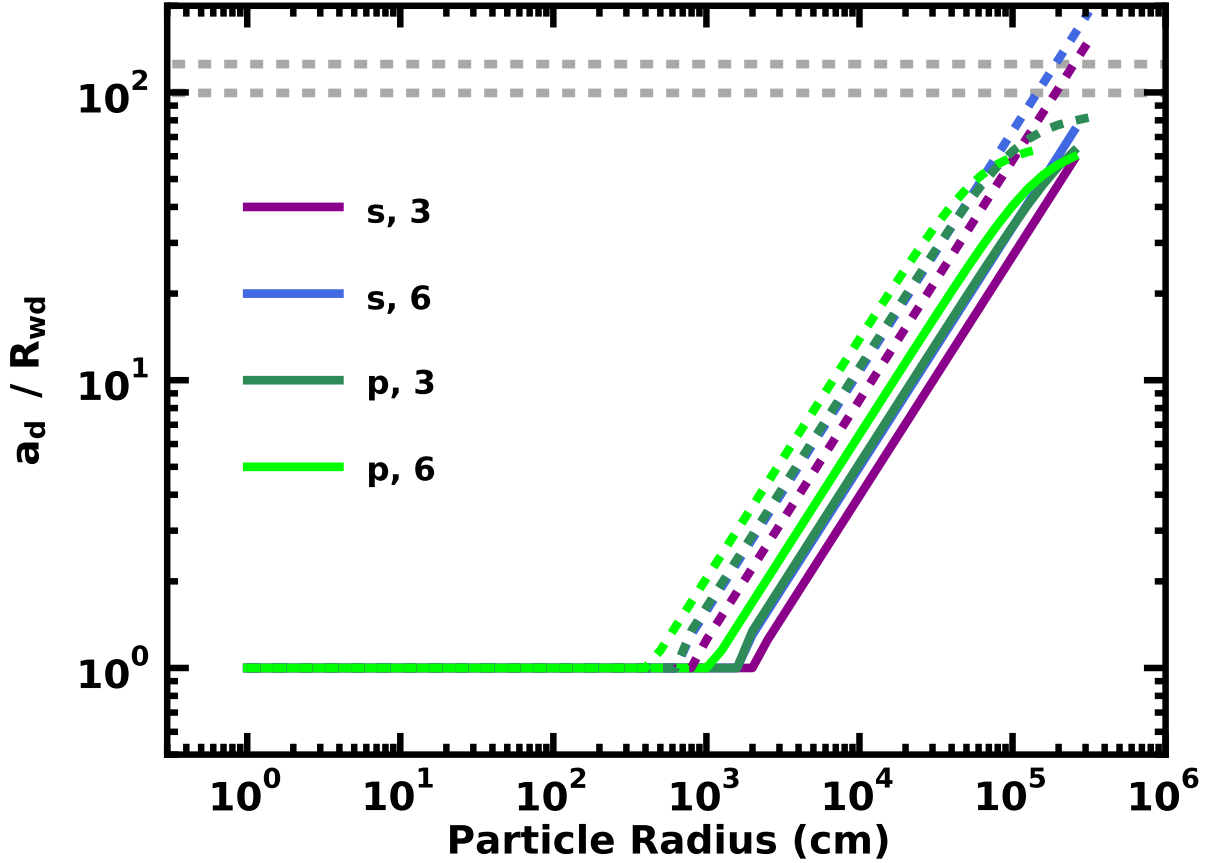


Fig. 1.— Innermost stable orbits for solid particles with cohesive strength orbiting a white dwarf with a mass of $0.6 M_{\odot}$ and a radius of $1.4 R_{\oplus}$. The solids have rotational periods equal to their orbital periods. Dashed horizontal grey lines indicate the Roche limit for fluids with $\rho = 3 \text{ g cm}^{-3}$ and 6 g cm^{-3} . As indicated in the legend, colored lines indicate results for spherical (‘s’) or prolate (‘p’, 2:1:1) particles with mean density $\rho = 3$ or 6 g cm^{-3} . Particles with radii smaller than 10 m (1 km) are stable against tidal disruption at the surface of the white dwarf (at $a \leq 40 R_{wd}$).

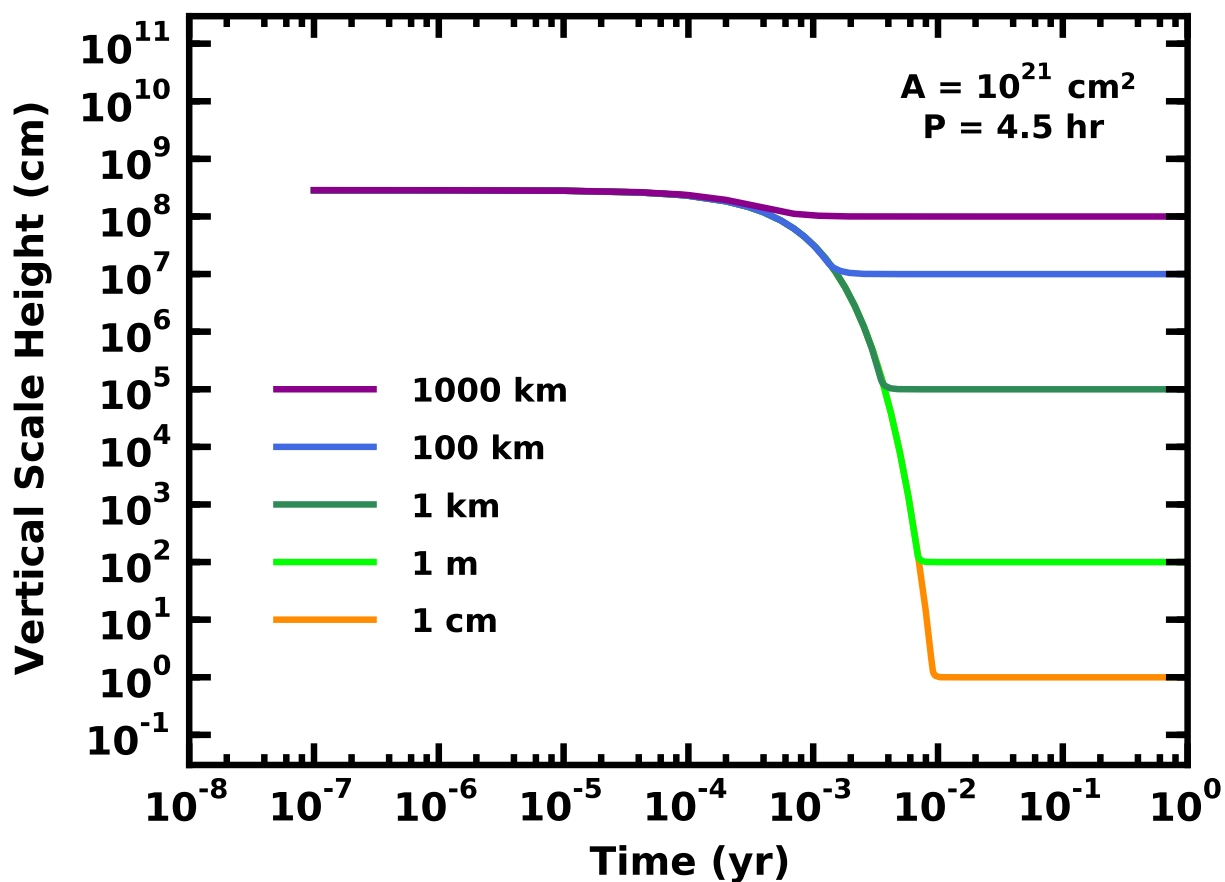


Fig. 2.— Eccentricity decay from collisional damping for swarms of indestructible mono-disperse solids with total cross-sectional area $A = 10^{21} \text{ cm}^2$ and orbital period $P = 4.5 \text{ hr}$ around a $0.6 M_{\odot}$ white dwarf. All swarms decay on the same time scale to equilibrium eccentricities and vertical scale heights that scale with the particle size, $e_{eq} \approx 1.7 \times 10^{-11}$ ($r/1 \text{ cm}$) and $H \approx r$.

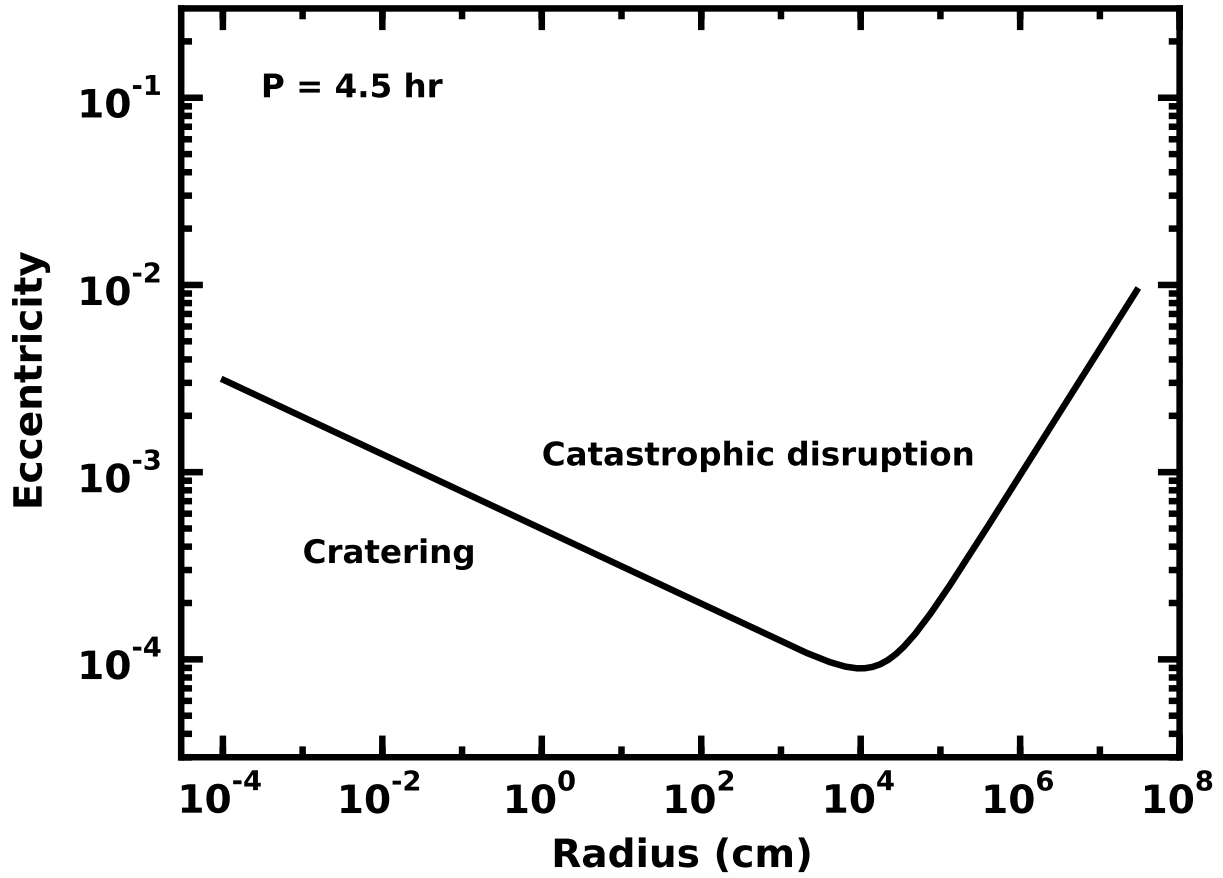


Fig. 3.— Critical eccentricity, e_c for catastrophic disruption. Collisions between equal mass objects with $e \geq e_c$ eject more than half of the total mass in debris. When $e < e_c$, collisions eject less mass and may produce a larger merged object.

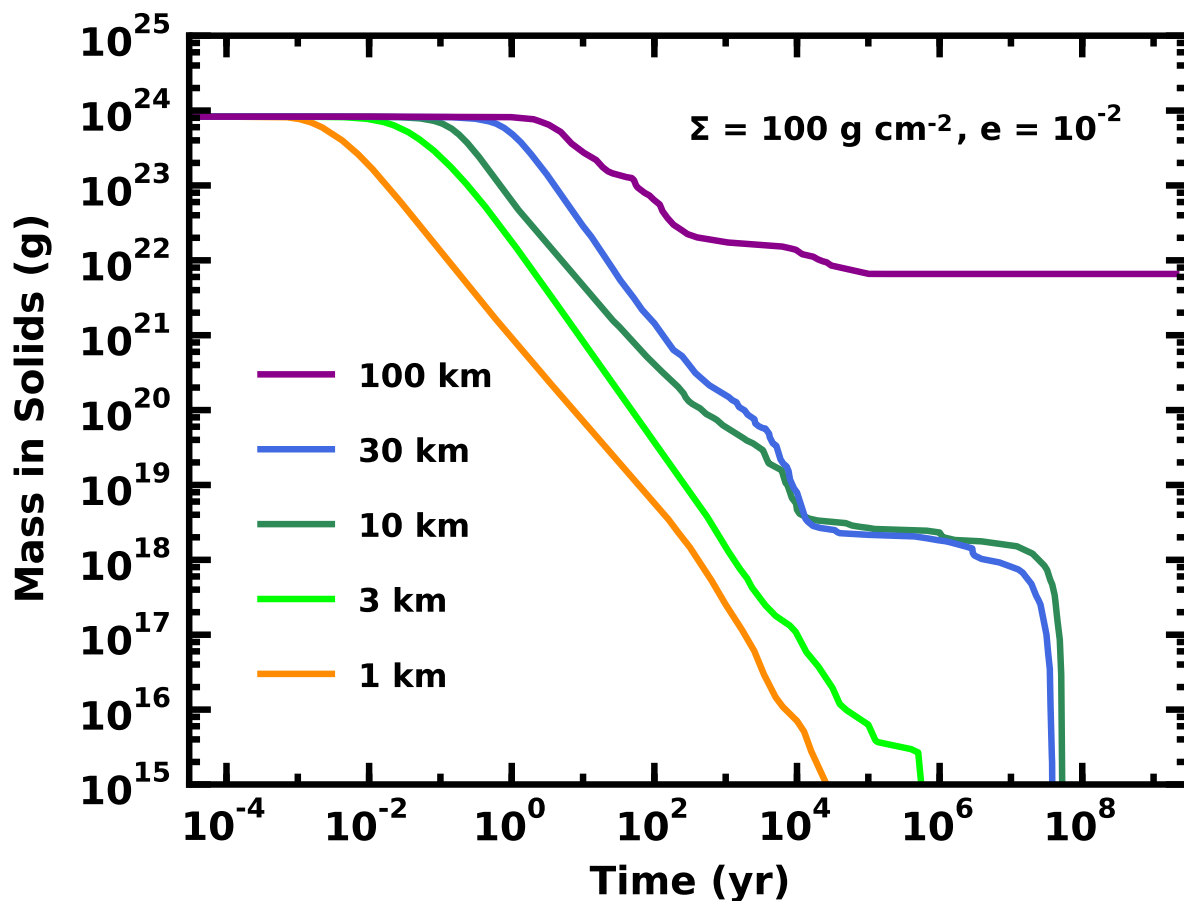


Fig. 4.— Time evolution of the mass of initially mono-disperse swarms of solid particles orbiting a $0.6 M_{\odot}$ white dwarf with initial surface density $\Sigma_0 = 100 \text{ g cm}^{-2}$ and eccentricity $e = 0.01$. The legend associates the solid curves with the initial radius r_0 of the largest object. As each system evolves, destructive collisions remove mass from the system. For $r_0 \leq 30 \text{ km}$, the mass drops rapidly to very low levels in $10^2 - 10^4 \text{ yr}$. When $r_0 = 100 \text{ km}$, the cascade gradually reduces the swarm to a single 100 km object, which has no collisions after roughly 0.1 Myr.

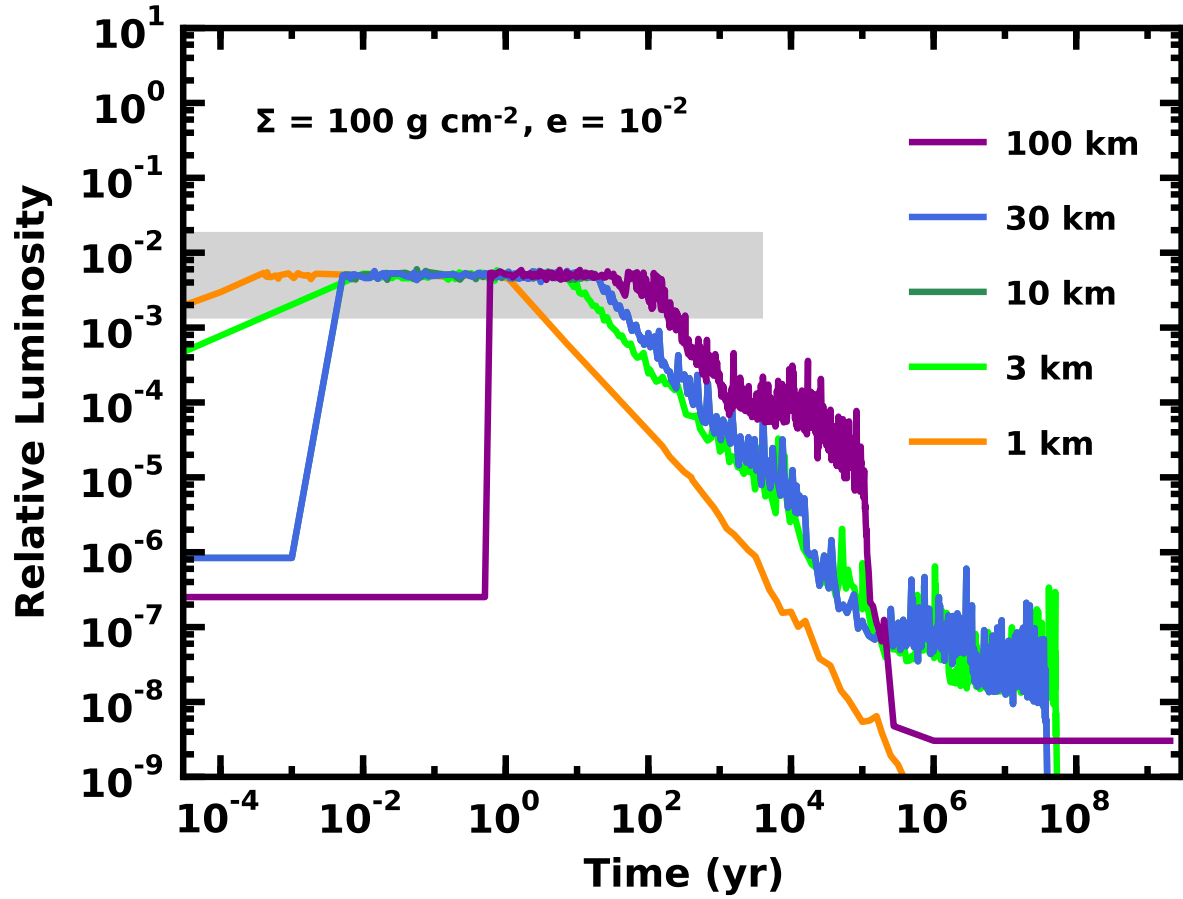


Fig. 5.— As in Fig. 4 for the reprocessed luminosity. The horizontal grey bar indicates the typical luminosity for the IR excesses of metallic line white dwarfs. After an initial spike of debris production, the luminosity drops to undetectable levels in 10^4 yr or less. Systems where the initial r_{max} is smaller decline more rapidly. Shot noise in collision rates produces fluctuations in the luminosity.

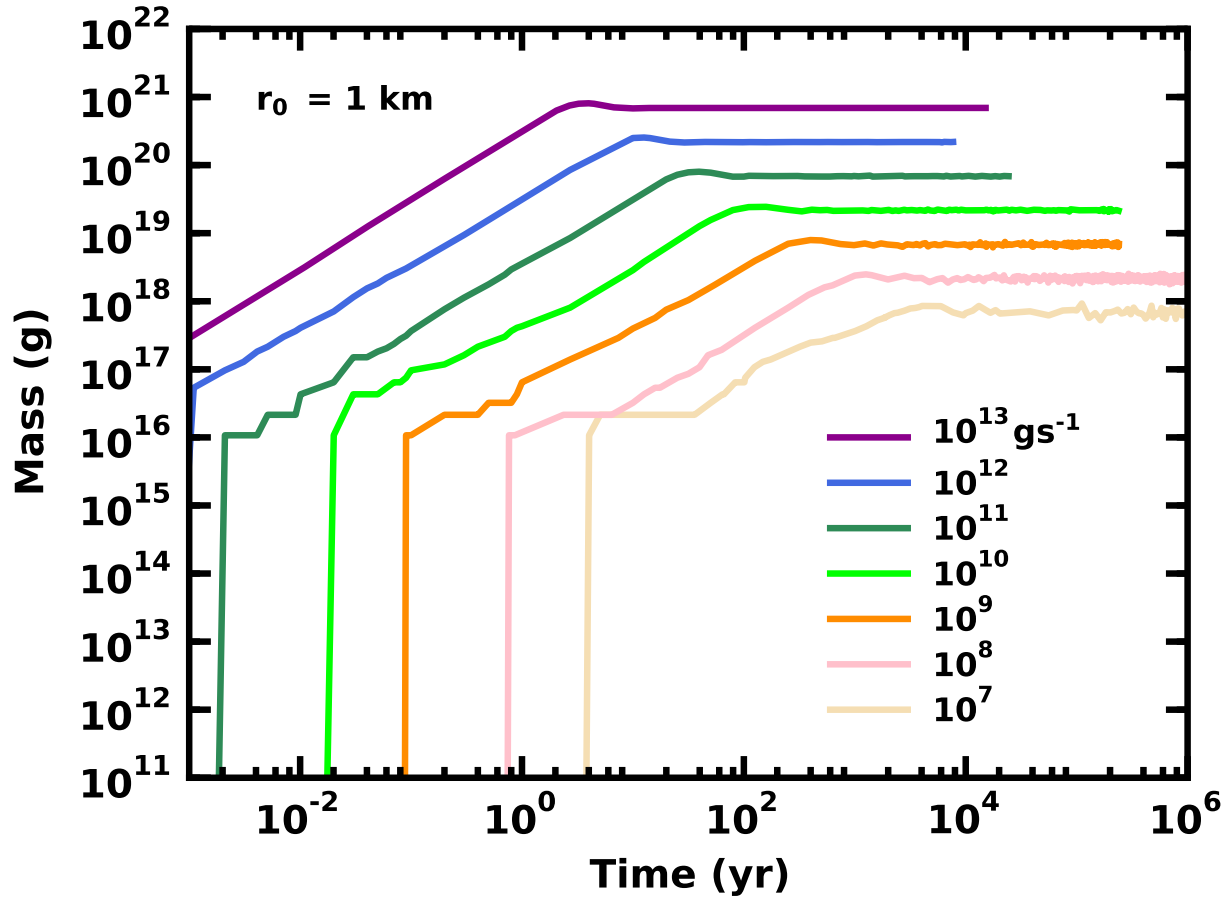


Fig. 6.— Time evolution of the mass in solids for systems with zero initial mass where 1 km particles are added at rates indicated in the legend. All systems reach an equilibrium mass $M_{d,eq}$ which depends on the input rate \dot{M}_0 ; fluctuations about $M_{d,eq}$ grow with decreasing \dot{M}_0 .

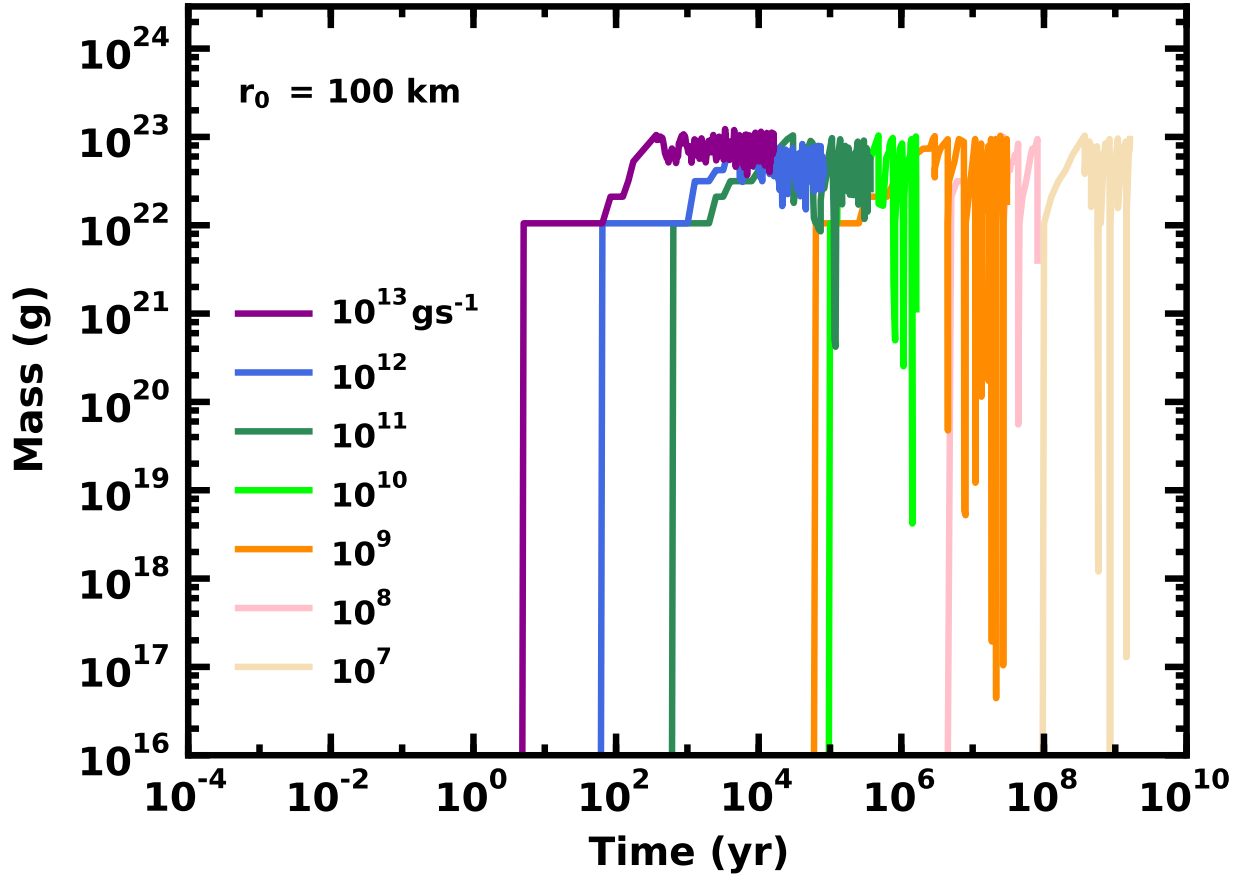


Fig. 7.— As in Fig. 6 for swarms with $r_{max} = 100 \text{ km}$. In swarms with very large solids ($r \gtrsim 100 \text{ km}$), all systems with input $\dot{M} = 10^7 - 10^{13} \text{ g s}^{-1}$ reach roughly the same maximum mass. Fluctuations in the mass grow with decreasing input \dot{M} .

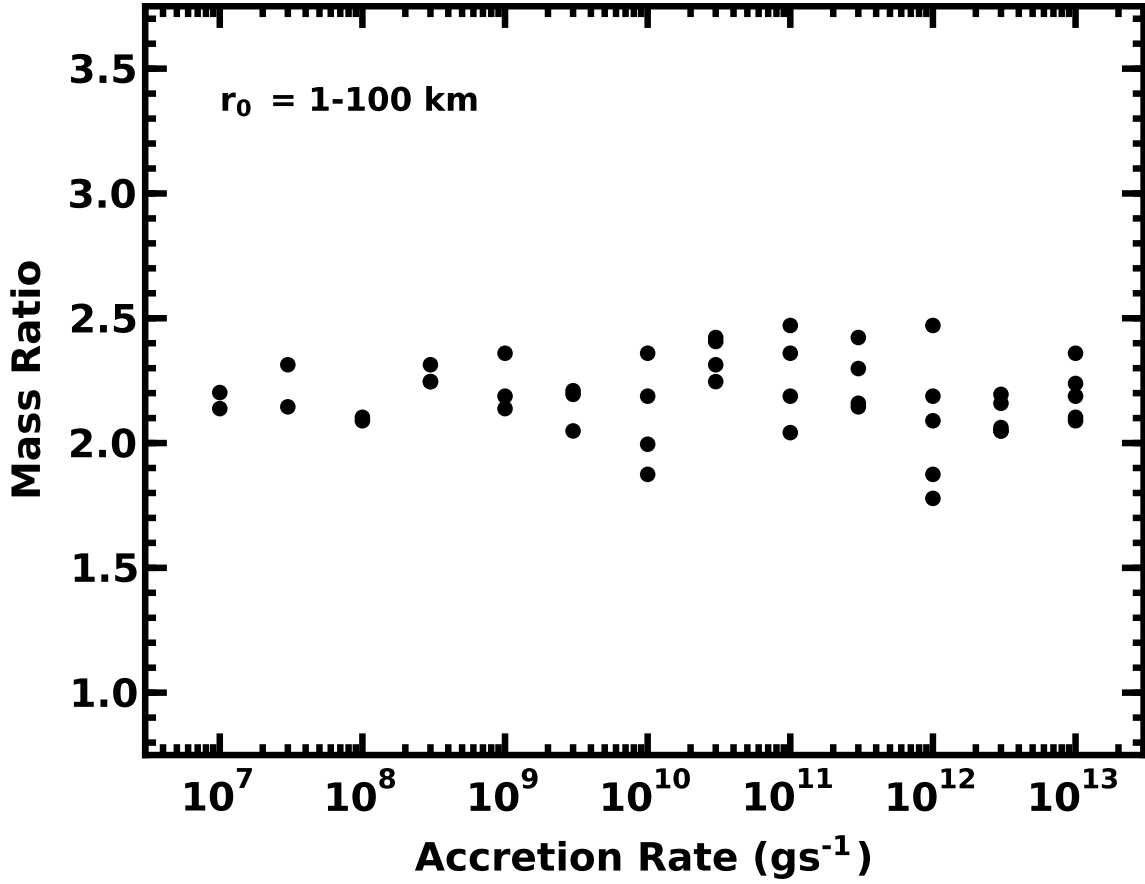


Fig. 8.— Variation of the mass ratio $\xi = M_{eq,n}/M_{d,eq}$ as a function of \dot{M}_0 for calculations with $r_0 = 1\text{--}100$ km. Although the equilibrium mass derived in the numerical simulations is somewhat more than a factor of two larger than the analytical prediction, the calculations match the variation of the equilibrium mass with \dot{M}_0 and r_0 .

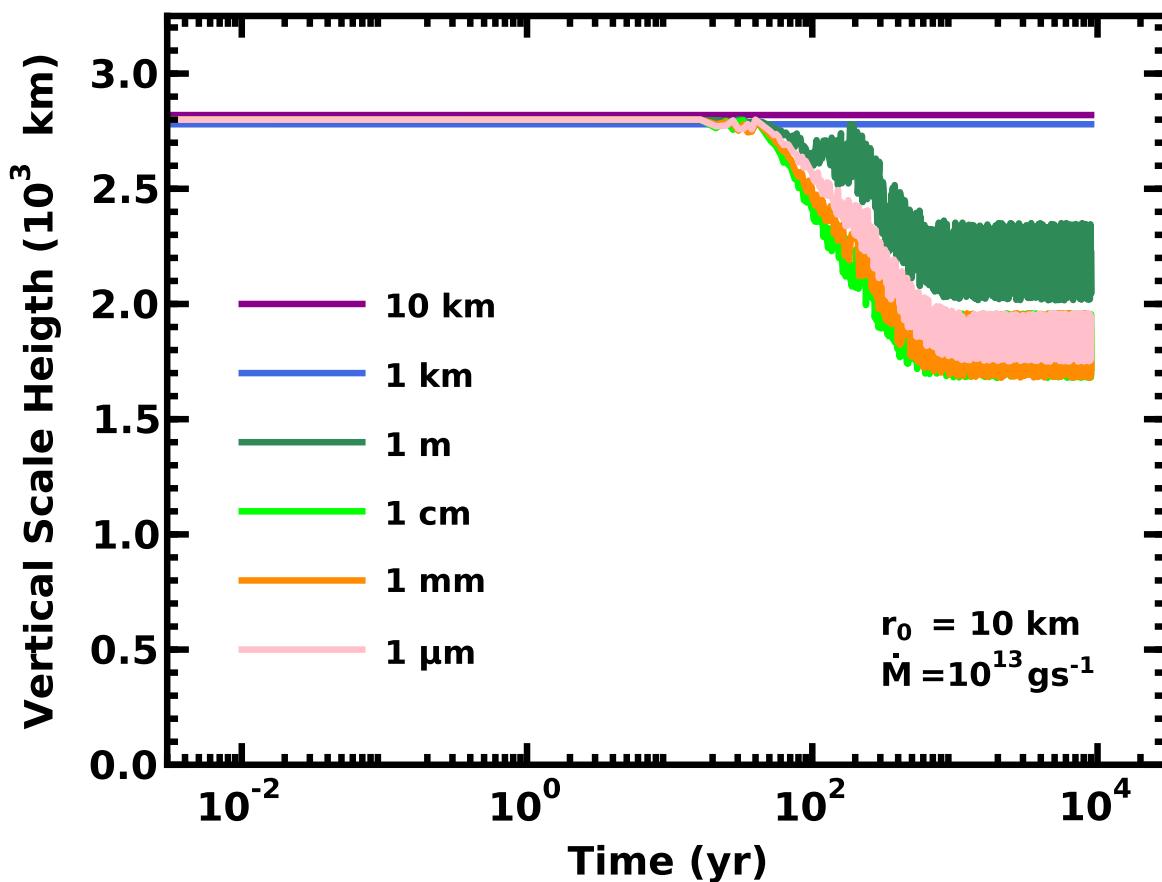


Fig. 9.— Time variation of the vertical scale height as a function of particle size for a calculation with $r_0 = 10$ km and $\dot{M}_0 = 10^{13}$ g s $^{-1}$. Particle sizes are indicated in the legend. As the mass in the annulus increases from zero at $t = 0$ to 7×10^{21} g at $t = 40$ – 50 yr, collisional damping is ineffective. Once the mass in solids reaches equilibrium, damping gradually reduces the vertical scale height for particles with $r \lesssim 10$ m. Damping is most effective for $r \approx 1$ – 10 mm.

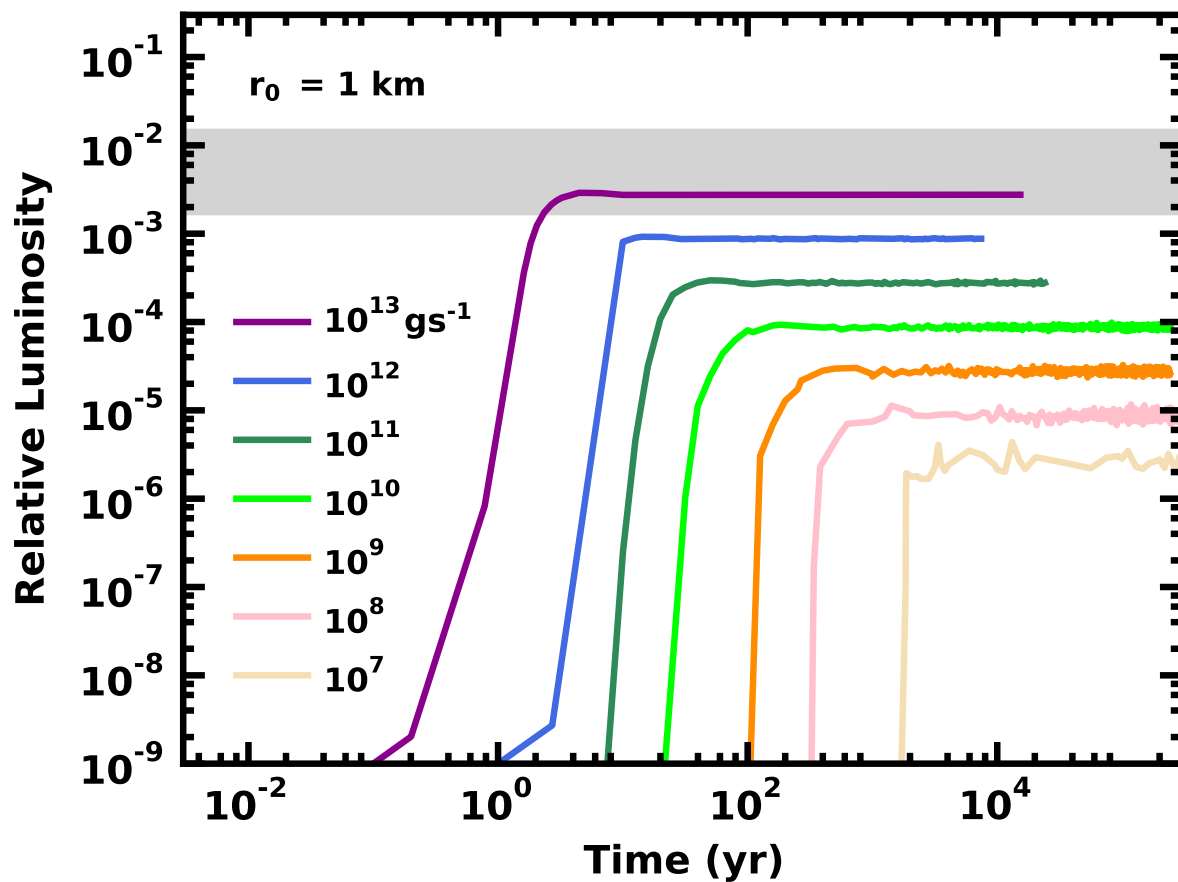


Fig. 10.— Evolution of the reprocessed luminosity for swarms of solids with an initial mass of zero, $r_{max} = 1$ km, and various input \dot{M} as indicated in the legend. The grey bar indicates the observed range of L_d/L_{wd} for white dwarfs with infrared excess emission. Although all systems reach a plateau luminosity which scales with \dot{M} , only systems with $\dot{M} \gtrsim 10^{12} \text{ g s}^{-1}$ achieve L_d/L_{wd} close to observed limits. Shot noise in the collision rates generate fluctuations about the plateau luminosity. Systems with smaller \dot{M} have larger fluctuations.

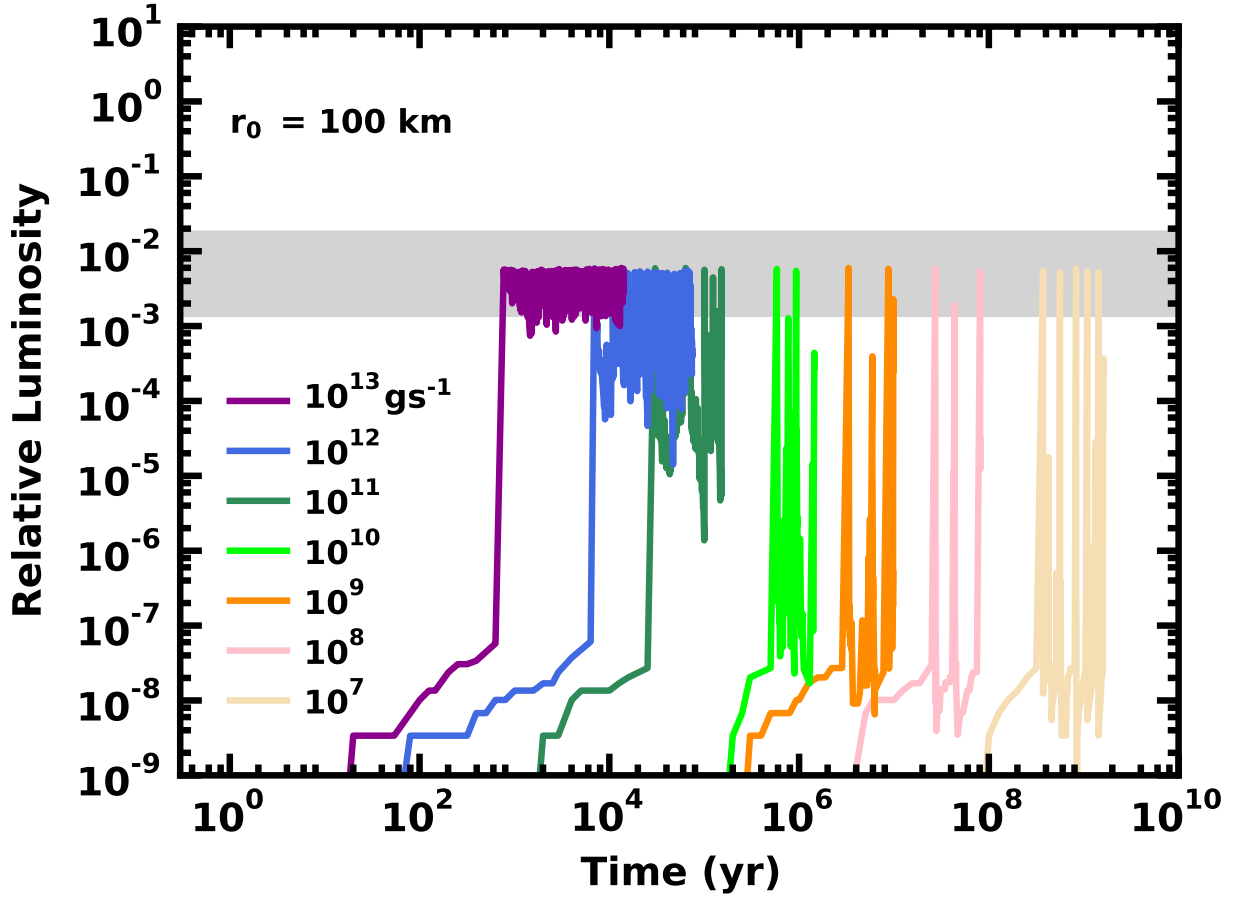


Fig. 11.— As in Fig. 10 for swarms with $r_{max} = 100$ km. For any $\dot{M} = 10^7 - 10^{13}$ g s^{-1} , collision cascades occasionally generate enough small particles to match typical observed luminosities. The fraction of time spent above $L_d/L_{wd} \gtrsim 10^{-3}$ scales with the input \dot{M} .

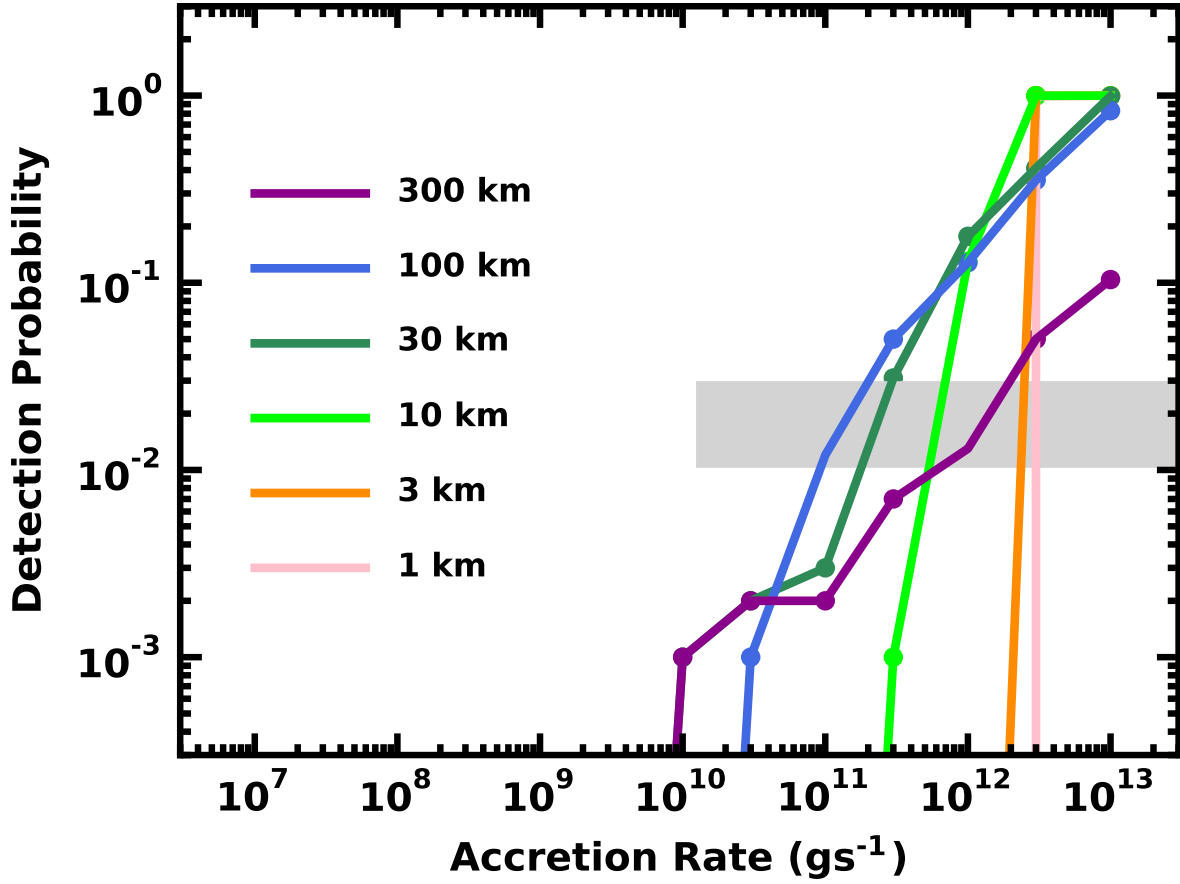


Fig. 12.— Detection probability (fraction of time with $L_d/L_{wd} \gtrsim 10^{-3}$) as a function of \dot{M}_0 for various r_0 listed in the legend. The grey horizontal bar indicates the observed frequency of debris disks around metallic line white dwarfs. Input accretion rates $\dot{M}_0 \approx 10^{11} - 10^{12} \text{ g s}^{-1}$ yield a detection probability comparable with the observed rate.